Journal of Inorganic Biochemistry 248 (2023) 112363

Contents lists available at ScienceDirect

Journal of Inorganic Biochemistry

journal homepage: www.elsevier.com/locate/jinorgbio

Synthesis, characterization, biomolecular interactions, molecular docking, and in vitro and in vivo anticancer activities of novel ruthenium(III) Schiff base complexes

Milica Međedović [a], Aleksandar Mijatović [b], Rada Baošić [c], Dejan Lazić [d], Žiko Milanović [e], Zoran Marković [e], Jelena Milovanović [f], Dragana Arsenijević [g], Bojana Stojanović [h], Miloš Arsenijević [d], Marija Milovanović [i], Biljana Petrović [a], Ana Rilak Simović [e,*]

[a] University of Kragujevac, Faculty of Science, Department of Chemistry, Radoja Domanovića 12, 34000 Kragujevac, Serbia
[b] University of Belgrade, Faculty of Mining and Geology, Đušina 7, 11000 Belgrade, Serbia
[c] University of Belgrade, Faculty of Chemistry, Studentski trg 12-16, 11000 Belgrade, Serbia
[d] Department of Surgery, Faculty of Medical Sciences, University of Kraujevac, Svetozara Markovića 69, 34000 Kragujevac, Serbia
[e] University of Kragujevac, Institute for Information Technologies Kragujevac, Department of Natural Sciences, Jovana Cvijića bb, 34000 Kragujevac, Serbia
[f] Departement of Histology and Embryology, Faculty of Medical Sciences, University of Kragujevac, 34000 Kragujevac, Serbia
[g] Departement of Pharmacy, Faculty of Medical Sciences, University of Kragujevac, 34000 Kragujevac, Serbia
[h] Departement of Patophysiology, Faculty of Medical Sciences, University of Kragujevac, 34000 Kragujevac, Serbia
[i] Center for Molecular Medicine and Stem Cell Research, Faculty of Medical Sciences, University of Kragujevac, 34000 Kragujevac, Serbia

ARTICLE INFO

Keywords:
Ruthenium(III)
Schiff bases
Biomolecular interactions
Docking simulations
Lewis lung cancer
Metastases

ABSTRACT

In order to discover new anticancer drugs, novel ruthenium(III) complexes [Ru(*L*)Cl(H_2O)], where L is tetradentate Schiff base *bis*(acetylacetone)ethylendiimine (acacen, **1**), *bis*(benzoylacetone)ethylendiimine (bzacen, **2**), (acetylacetone)(benzoylaceton)ethylendiimine (acacbzacen, **3**), *bis*(acetylacetone)propylendiimine (acacpn, **4**), *bis*(benzoylacetone)propylendiimine (bzacpn, **5**) or (acetylacetone)(benzoylaceton)propylendiimine (acacbzacpn, **6**), were synthesized. The complexes **1 – 6** were characterized by elemental analysis, molar conductometry, and by various spectroscopic techniques, such as UV–Vis, IR, EPR, and ESI-MS. Based on in vitro DNA/BSA experiments, complexes **2** (bzacen) and **5** (bzacpn) with two aromatic rings showed the highest DNA/BSA-activity, suggesting that the presence of the aromatic ring on the tetradentate Schiff base ligand contributes to increased activity. Moreover, these two compounds showed the highest cytotoxic effects toward human, A549 and murine LLC1 lung cancer cells. These complexes altered the ratio of anti- and pro-apoptotic molecules and induced apoptosis of A549 cells. Further, complexes **2** and **5** reduced the percentage of Mcl1 and Bcl2 expressing LLC1 cells, induced their apoptotic death and exerted an antiproliferative effect against LLC1. Finally, complex **5** reduced the volume of mouse primary heterotopic Lewis lung cancer, while complex **2** reduced the incidence and mean number of metastases per lung. Additionally, molecular docking with DNA revealed that the reduced number of aromatic rings or their absence causes lower intercalative properties of the complexes in order: **2 > 5 > 6 > 3 > 4 > 1**. It was observed that conventional hydrogen bonds and hydrophobic interactions contribute to the stabilization of the structures of complex-DNA. A molecular docking study with BSA revealed a predominance of **1 – 6** in binding affinity to the active site III, a third *D*-shaped hydrophobic pocket within subdomain IB.

Abbreviations: acacbzacen, (acetylacetone)(benzoylaceton)ethylendiimine;; acacbzacpn, (acetylacetone)(benzoylaceton)propylendiimine;; acacen, *bis*(acetylacetone)ethylendiimine;; acacpn, *bis*(acetylacetone)propylendiimine;; bzacen, *bis*(benzoylacetone)ethylendiimine;; A549, human lung cancer cell line;; A549cisR, cisplatin resistant human lung cancer cell line;; Bcl2, B-cell lymphoma 2;; bzacpn, (benzoylaceton)propylendiimine;; HCT116 and CT26, colorectal cancer cell line;; HuH-7, hepatocyte-derived carcinoma cell line;; LLC1, murin Lewis lung cancer cell line;; MCF-7, breast cancer cell line;; Mcl, mantle cells lymphoma;; TK10, renal cancer cell line;; UACC62, melanoma cancer cell line.

* Corresponding author.
E-mail address: anarilak@kg.ac.rs (A.R. Simović).

https://doi.org/10.1016/j.jinorgbio.2023.112363
Received 14 July 2023; Received in revised form 25 August 2023; Accepted 28 August 2023
Available online 29 August 2023

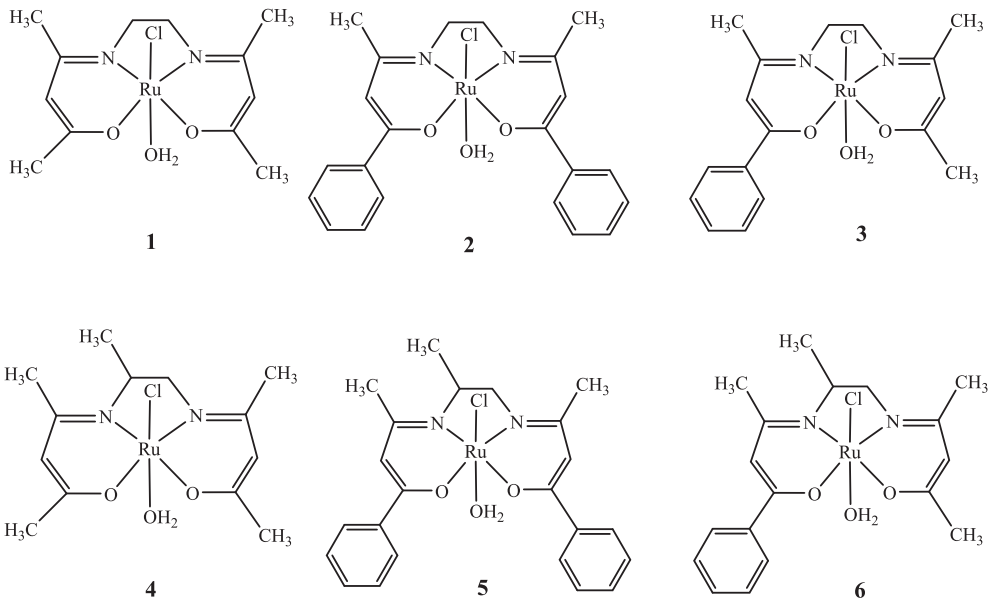

Fig. 1. Ru(III)-Schiff base complex structures.

1. Introduction

Transition metal complexes containing Schiff bases have attracted considerable attention because of their diverse uses, including synthesis, catalytic reactions, and medicinal chemistry [1]. Schiff bases have been extensively investigated because of their selectivity and sensitivity to the central metal atom, synthetic flexibility, and structural analogies with natural biological molecules. Schiff bases with imine or azomethine groups and their complexes have been employed as medicines with a variety of biological activity, including anticancer, antioxidant, antifungal, antibacterial and diuretic properties. They possess a wide range of biochemical, clinical, and pharmacological features. The presence of an imine group in such complexes has been proven to be essential for their biological actions. Moreover, they are found in a variety of natural, naturally produced, and non-natural materials and are important in understanding the biological mechanisms of transformation and racemization reactions [2].

Scientists working in this field aim to design a compound based on ruthenium that outperforms the most widely used metallotherapeutic, cisplatin, in terms of effectiveness, toxicity, lack of cross-resistance, or pharmacological properties. Organometallic compounds with unique properties that intermediate between those of classical inorganic and organic materials open up new avenues for medicinal chemistry and the development of new therapeutic agents. Furthermore, tetradentate ruthenium complexes bearing symmetrical and asymmetrical *bis*-type Schiff bases comprising aliphatic and aromatic 1,2-diamines and various aldehydes/ketones are becoming increasingly important in the creation of complexes relating to synthetic and natural oxygen carriers [3,4]. In 2015, Ajibade et al. reported new mononuclear Ru(III) complexes containing tetradentate N_2O_2 Schiff bases generated from ethane-1,2-diamine, 4-acetylresorcinol, acetylacetone and 1-phenylbutane-1,3-dione. These complexes showed moderate to strong DPPH and ABTS radical scavenging activities. Additionally, the antitumor effects of Ru (III) compounds were examined against several human cancers: breast cancer (MCF-7), melanoma cancer (UACC62) and renal cancer cells (TK10). These complexes showed a low to moderate antiproliferative effect against the selected tumors [5]. Recently, Subarkhan et al. described the synthesis and biological activity of tetranuclear organometallic Ru-Schiff base compounds. They reported higher activity of Ru complexes against several human cancer cell lines (i.e., LoVo, HuH-7, MCF-7, A549, and A549cisR) compared to cisplatin. Moreover, Ru complexes showed significantly decreased IC50 values (3.39 ± 0.5 and 5.70 ± 0.3 mM, respectively) for cisplatin-resistant A549cisR cells than cisplatin (17.24 ± 1.5 mM), implying that Ru complexes have the capacity to overcome cisplatin-induced drug resistance [6].

In continuation of our efforts toward the design of organometallic compounds as potential chemotherapeutic agents, we have synthesized and characterized the new series of mononuclear Ru(III)-Schiff base complexes of the general formula [Ru(*L*)Cl(H_2O)] where L = *bis*(acetylacetone)ethylendiimine (acacen, **1**), *bis*(benzoylacetone)ethylendiimine (bzacen, **2**), (acetylacetone)(benzoylaceton)ethylendiimine (acacbzacen, **3**), *bis*(acetylacetone) propylendiimine (acacpn, **4**), *bis* (benzoylacetone)propylendiimine (bzacpn, **5**) or (acetylacetone) (benzoylaceton)propylendiimine (acacbzacpn, **6**). The biomolecular interactions of **1–6** with calf thymus DNA (CT DNA) and bovine serum albumin (BSA), and in vitro antitumor activity against human and mouse cell lines of lung adenocarcinoma (A549 and LLC1) and colorectal cancer (HCT116 and CT26) were described, respectively. Finally, in vivo activity of **2** and **5** was performed on a heterotopic model of murine Lewis lung cancer (LLC1 cells). The structures of the newly synthesized Ru complexes **1–6** are presented in Fig. 1.

2. Experimental

2.1. Materials and methods

Sodium salt of deoxyribonucleic acid from calf thymus (CT-DNA), bovine serum albumin (BSA), ruthenium(III) chloride ($RuCl_3{\cdot}3H_2O$), Hoechst 33258, ethidium bromide (EB), ibuprofen and eosin Y were commercially available (Sigma Aldrich). Schiff base ligands *bis*(acetylacetone)ethylendiimine (acacen), *bis*(benzoylacetone)ethylendiimine (bzacen), (acetylacetone)(benzoylaceton)ethylendiimine (acacbzacen), *bis*(acetylacetone)propylendiimine (acacpn), *bis*(benzoylacetone)propylendiimine (bzacpn) or (acetylacetone)(benzoylaceton)propylendiimine (acacbzacpn) were prepared according to the literature's instructions [7]. Their ^1H and ^{13}C NMR spectra are presented in Figs. S1 and S2. Phosphate buffer (PBS, 10 mM, C_{NaCl} = 137 mM, C_{KCl} = 2.7 mM, pH = 7.4) was purchased from Sigma Aldrich. The stock solution of CT DNA was prepared in PBS, which gave a ratio of the UV absorbances at 260 and 280 nm (A_{260}/A_{280}) between 1.8 and 1.9, suggesting that the DNA solution was free of proteins. The DNA concentration was determined by UV absorbance at 260 nm ($\varepsilon = 6600\ M^{-1}\ cm^{-1}$) [8]. BSA stock

solution was prepared by dissolving the solid in PBS at pH = 7.4 and keeping the solution concentration constant at 2 μM. All prepared solutions were kept at 4 °C and consumed within 5 days.

The UV–Vis spectra were acquired using 1.0 path-length quartz cuvettes (3.0 mL) on a Perkin-Elmer Lambda 35 double beam spectrophotometer. Perkin-Elmer 983 G spectrometer was used to record infrared spectra. NMR signals were referenced to residual proton or carbon signals of the deuterated solvent (^{1}H and ^{13}C NMR) and reported in ppm relative to TMS. Electrospray ionization mass spectra were performed on the LTQ Orbitrap XL. The Shimadzu RF-1501 PC spectrofluorometer was used to measure fluorescence. Viscosity measurements were performed using an Ubbelodhe viscometer thermostated at 25 ± 0.1 °C. Molar conductances of the Ru complexes **1–6** were measured on freshly prepared 10^{-3} M solutions in dimethylformamide at room temperature using a Crison EC-Meter Basic 30+ conductivity cell. Electron paramagnetic resonance (EPR) experiments were carried out using an X-band MagnetTech MS300 spectrometer with a nominal frequency of 9.5 GHz. Furthermore, the microwave power was 3.16 mW (microwave attenuation 15 dB), with a modulation amplitude of 0.2 mT [9].

2.2. General synthetic method for [Ru(L)Cl(H$_2$O)] (1–6)

$RuCl_3{\cdot}3H_2O$ in the appropriate amount (0.3825 mmol) was dissolved in ethanol. The solution was refluxed for approximately 2 h until the color of the solution changed from brown to green. The appropriate amounts of Schiff bases (1 mmol) were then added, and the reflux process continued for 5 h. The color of the solutions changed to a brow or brown-reddish over this period. The products were obtained as a dark brown solid through rotary concentration under reduced pressure to ca. ¼ of the initial volume. The complexes were collected by filtration and dried under vacuum after being washed with ethanol and diethyl ether.

[Ru(acacen)Cl(H$_2$O)] (**1**). 100.0 mg (0.3825 mmol) of $RuCl_3{\cdot}3H_2O$ and 85,79 mg (0.3825 mmol) of *bis*(acetylacetone)ethylendiimine in 20 mL of ethanol afforded **1** as a brown solid. Yield: 75.3 mg (75.3%). Anal Calcd for $C_{12}H_{20}ClN_2O_3Ru$ (376.82): C, 38.25; H, 5.35; N, 7.43. Found: C, 38.21; H, 5.29; N, 7.47. Complex **1** is soluble in DMSO and slightly soluble in water, methanol, ethanol, acetone, chloroform, dichloromethane, and acetonitrile. Selected IR (KBr, cm^{-1}): $\nu_{(O—H)}$ 3445 (m); $\nu_{(C=C)}$ 1622 (m), 1594 (m); $\nu_{(CH=N)}$ 1540 (s); $\nu_{(C—O)}$ 1325 (s). UV/Vis spectrum (DMSO; λ_{max}, nm (ε, M^{-1} cm^{-1})): 259(), 324 (59139), 408 (21731). ESI-MS: $[Ru(acacen)]^+$ (*m/z* = 324.04).

[Ru(bzacen)Cl(H$_2$O)] (**2**). 100.0 mg (0.3825 mmol) of $RuCl_3{\cdot}3H_2O$ and 133,1 mg (0.3825 mmol) of *bis*(benzoylacetone)ethylendiimine in 20 mL of ethanol afforded **2** as a brown solid. Yield: 82.5 mg (82.5%). Anal Calcd for $C_{22}H_{24}ClN_2O_3Ru$ (500.97): C, 52.75; H, 4.83; N, 5.59. Found: C, 52.78; H, 4.87; N, 5.58. Complex **2** is soluble in DMSO and slightly soluble in water, methanol, ethanol, acetone, chloroform, dichloromethane, and acetonitrile. Selected IR (KBr, cm^{-1}): $\nu_{(O—H)}$ 3445 (m); $\nu_{(C=C)}$ 1595 (m), 1540 (m); $\nu_{(CH=N)}$ 1502 (s), 1486 (s), 1447 (s); $\nu_{(C—O)}$ 1362 (s), 1274 (s). UV/Vis spectrum (DMSO; λ_{max}, nm (ε, M^{-1} cm^{-1})): 262 (49028), 313 (30301), 409 (18570). ESI-MS: $[Ru(bzacen)(H_2O)]^+$ (*m/z* = 466.08); $[Ru(bzacen)]^+$ (m/z = 448.07).

[Ru(acacbzacen)Cl(H$_2$O)] (**3**). 100.0 mg (0.3825 mmol) of $RuCl_3{\cdot}3H_2O$ and 109,5 mg (0.3825 mmol) (acetylacetone)(benzoylaceton)ethylendiimine in 20 mL of ethanol afforded **3** as a brown solid. Yield: 69.8 mg (69.8%). Anal Calcd for $C_{17}H_{22}ClN_2O_3Ru$ (439.89): C, 46.52; H, 5.05; N, 6.38. Found: C, 46.54; H, 5.12; N, 6.34. Complex **3** is soluble in DMSO and slightly soluble in water, methanol, ethanol, acetone, chloroform, dichloromethane and acetonitrile. Selected IR (KBr, cm^{-1}): $\nu_{(O—H)}$ 3444 (m); $\nu_{(C=C)}$ 1621 (m), 1595 (m); $\nu_{(CH=N)}$ 1540 (s), 1502 (s); $\nu_{(C—O)}$ 1326 (s). UV/Vis spectrum (DMSO; λ_{max}, nm (ε, M^{-1} cm^{-1})): 269 (45233), 325 (49707), 410 (20120). ESI-MS: $[Ru(acacbzacen)(H_2O)]^+$ (*m/z* = 404.06); $[Ru(acacbzacen)]^+$ (m/z = 386.05).

[Ru(acacpn)Cl(H$_2$O)] (**4**). 100.0 mg (0.3825 mmol) of $RuCl_3{\cdot}3H_2O$ and 91,2 mg (0.3825 mmol) of *bis*(acetylacetone)propylendiimine in 20 mL of ethanol afforded **4** as a brown solid. Yield: 72.1 mg (72.1%). Anal Calcd for $C_{13}H_{22}ClN_2O_3Ru$ (390.85): C, 39.95; H, 5.67; N, 7.17. Found: C, 39.92; H, 5.69; N, 7.11. Complex **4** is soluble in DMSO and slightly soluble in water, methanol, ethanol, acetone, chloroform, dichloromethane, and acetonitrile. Selected IR (KBr, cm^{-1}): $\nu_{(O—H)}$ 3445 (m); $\nu_{(C=C)}$ 1621 (m); $\nu_{(CH=N)}$ 1521 (s); $\nu_{(C—O)}$ 1332 (s). UV/Vis spectrum (DMSO; λ_{max}, nm (ε, M^{-1} cm^{-1})): 269 (55642), 324 (59109), 403 (24896). ESI-MS: $[Ru(acacpn)(H_2O)]^+$ (*m/z* = 355.07); $[Ru(acacpn)]^+$ (m/z = 338.05).

[Ru(bzacpn)Cl(H$_2$O)] (**5**). 100.0 mg (0.3825 mmol) of $RuCl_3{\cdot}3H_2O$ and 138.6 mg (0.3825 mmol) of *bis(*benzoylacetone)propylendiimine in 20 mL of ethanol afforded **5** as a brown solid. Yield: 87.2 mg (87.2%). Anal Calcd for $C_{23}H_{26}ClN_2O_3Ru$ (514.99): C, 53.64; H, 5.09; N, 5.44. Found: C, 53.67; H, 5.11; N, 5.41. Complex **5** is soluble in DMSO and slightly soluble in water, methanol, ethanol, acetone, chloroform, dichloromethane, and acetonitrile. Selected IR (KBr, cm^{-1}): $\nu_{(O—H)}$ 3438 (m); $\nu_{(C=C)}$ 1595 (s); $\nu_{(CH=N)}$ 1502 (s), 1486 (s); $\nu_{(C—O)}$ 1339 (s). UV/Vis spectrum (DMSO; λ_{max}, nm (ε, M^{-1} cm^{-1})): 260 (53084), 316 (30758), 409 (19905). ESI-MS: $[Ru(bzacpn)(H_2O)]^+$ (*m/z* = 480.09).

[Ru(acacbzacpn)Cl(H$_2$O)] (**6**). 100.0 mg (0.3825 mmol) of $RuCl_3{\cdot}3H_2O$ and 114,9 mg (0.3825 mmol) of (acetylacetone)(benzoylaceton)propylendiimine in 20 mL of ethanol afforded **6** as a brown solid. Yield: 70.5 mg (70.5%). Anal Calcd for $C_{18}H_{24}ClN_2O_3Ru$ (452.92): C, 47.73; H, 5.34; N, 6.19. Found: C, 47.70; H, 5.40; N, 6.17. Complex **6** is soluble in DMSO and slightly soluble in water, methanol, ethanol, acetone, chloroform, dichloromethane, and acetonitrile. Selected IR (KBr, cm^{-1}): $\nu_{(O—H)}$ 3444 (m); $\nu_{(C=C)}$ 1596 (s); $\nu_{(CH=N)}$ 1503 (s), 1486 (s); $\nu_{(C—O)}$ 1333 (s). UV/Vis spectrum (DMSO; λ_{max}, nm (ε, M^{-1} cm^{-1})): 274 (18134), 324 (25339), 403 (9867). ESI-MS: $[Ru(acacbzacpn)(H_2O)]^+$ (*m/z* = 418.08); $[Ru(acacbzacpn)]^+$ (m/z = 400.07).

2.3. DNA-binding studies

Absorption spectroscopy investigations were conducted to evaluate a potential binding manner of compounds **1–6** to DNA and to quantify the strength of binding by calculating binding constants (K_b). The DNA measurements were monitored at 37 °C. By employing a fixed concentration of the complex (10 μM), to which increments of DNA solution were added, the absorption titration of ruthenium(III) complexes in 10 mM buffer solution (pH = 7.4) was carried out.

Fluorescence spectroscopy was used to examine the competitive binding interactions between ethidium bromide (EB) and Hoechst 33258 and complexes **1–6** with CT DNA. For EB and Hoechst 33258, the excitation and emission wavelengths were set at 527 and 346 nm and 612 and 490 nm, respectively, to measure the fluorescence intensities. In 10 mM PBS buffer (pH = 7.4), stock solutions of complexes (0.1 mM) and CT DNA (2.0 mM) were prepared. At room temperature, titration studies were conducted by adding microliter quantities (40 μL) of a stock solution of the complex to the DNA solution (2.0 mL) after an equilibration period of two minutes. The final DNA concentration for fluorescence analysis was 27.5 μM, while the concentration of complexes ranged from 5.5 μM to 55.0 μM. For EB experiments, the emission was measured between 550 and 750 nm, while for Hoechst 33258 experiments, it was measured between 370 and 650 nm, respectively.

In the presence of an increasing concentration of **1–6**, the viscosity of a DNA solution was observed. Six times for each sample, the flow time was monitored using a digital stopwatch, and the average flow time was determined. The results were shown as $(\eta/\eta_0)^{1/3}$ *vs.* r, where η is the viscosity of the DNA solution in the presence of complex, and η_0 is the viscosity of the DNA solution in buffer alone.

2.4. Albumin-binding studies

Tryptophan fluorescence quenching tests with BSA (2 μM) in PBS buffer (pH = 7.4) were used to conduct the protein binding investigation. Using complexes **1–6** as quenchers, the quenching of the emission

intensity of the tryptophan residues in BSA at 364 nm was noticed when the concentration of the quenchers (up to 2.0×10^{-5} M) increased. At a 285 nm excitation wavelength, fluorescence spectra in the 300–500 nm region were recorded. Under the same experimental circumstances, the fluorescence spectra of the compounds in buffered solution were recorded, but no fluorescence emission was detected. The strength of the interactions between complexes **1–6** and BSA has been determined, and the relevant constants have been calculated, using the Stern-Volmer and Scatchard equations (eqs. S3–S5, ESI) and graphs. Furthermore, we have conducted competitive BSA-interactions with the site markers eosin Y, which serves as a marker for site I of the subdomain IIA, and ibuprofen, which serves as a marker for site II of the subdomain IIIA. The fluorescence emission range was between 300 and 500 nm, with the excitation wavelength set at 295 nm. Equimolar amounts of BSA and markers (2.0×10^{-6} M) were added to the solutions. The Ru-Schiff base complexes **1–6** were added in increasing concentrations up to 2.0×10^{-5} M.

2.5. Molecular docking

A molecular docking investigation was conducted in addition to the experimental procedures based on UV–Vis and spectrofluorimetric techniques to thoroughly assess the investigated compounds' affinity for binding to DNA and BSA macromolecules. The Lamarckian Genetic Algorithm (LGA) and Autodock 4.2 software were used to determine the binding affinity of newly synthesized complexes toward the DNA and BSA macromolecules [10]. Maximum 250,000 energy assessments, 27,000 generations, and mutation and crossover rates of 0.02 and 0.8, respectively, were the parameters established for the LGA method used for protein-ligand rigid-flexible docking. Molecular docking simulation consists of several sequential stages, including ligand preparation, protein identification and preparation, as well as grid formation. Firstly, the Gaussian 16 software package was used to optimize the Ru complexes' structural characteristics [11] in conjunction with the B3LYP–D3BJ method and the 6–311 + G(d,p) basis set [12,13]' and def2-TZVPD, triple-zeta-valence, basis set for Ru (incorporating effective core potential). The 3D X-ray crystallographic structure of the BSA protein was obtained from RCSB Protein Data Bank using the PDB ID: 4F5S [14]. Only chain A was retained, while chain B, residual atoms, heteroatoms and water molecules were removed from the initial structure of BSA using BIOVA Discovery Studio 4.0. The search space of BSA was restricted to a grid box size of 60 × 60 × 60 Å with a grid spacing of 0.375 A following the XYZ dimensions: for site I (IIA): −4.80 × 30.50 × 101.01; for site II (IIIA): 10.91 × 16.30 × 119.72; for site III (IB): 19.86 × 33.53 × 97.92. On the other hand, the initial structure of canonical B-DNA (PDB ID: 1BNA) and DNA with an intercalation gap (PDB ID: 1Z3F) was retrieved from the RCSB Protein Data Bank [15,16] Grid box dimensions of 60 × 74 × 120 Å for the 1BNA structure were set at 15.81 × 21.31 × 9.88 Å with a grid spacing of 0.375 Å. In our earlier research, we described the standard techniques for choosing the additional docking parameters [17,18].

2.6. Cytotoxic activity

2.6.1. Cell culture

Cell lines of human lung cancer (A549, CCL-185™) and human colorectal cancer (HCT116, CCL-247™), murine Lewis lung cancer (LLC1, CRL-1642™) and murine colon cancer (CT26, CRL-2638™), cell lines of murine fibroblasts (3 T3, CRL-1658™) and human fibroblasts (MRC5, CCL-171™), all from the American Type Culture Collection, were grown in standard conditions. Only cell suspensions with >95% of viable cells, as determined by trypan blue staining, were used for the experiments.

2.6.2. MTT assay

The potential of **1–6** to reduce the viability of tumor cell lines was analyzed by MTT (3-(4,5-dimethylthiazol-2-yl)-2,5-diphenyltetrazolium bromide) colorimetric assay. A volume of 100 μL of suspension of cells (density of 5×10^4 cells/mL) was placed in 96-well plates. After cells adhered to the plastic (the following day), the culture medium was removed, and 100 μL of tested compounds, serially diluted two-fold in medium to concentrations ranging from 1000 to 7.8 μM, was added to each well. Cells in the medium with tested complexes were maintained in incubator at 37 °C with 5% CO_2 for 72 h. After completion of incubation, the medium was replaced with MTT solution and incubated for an additional four hours. The optical density of each well was detected on the microplate multimode detector Zenyth 3100 at 595 nm. The percentage of viable cells was determined using the formula: % of viable cells = (*E*-B)/(S—B) × 100, where B is for the background of medium alone, S is for total viability or spontaneous death of untreated target cells, and E is for the experimental well. Each experiment was done in triplicate and also repeated three times.

2.6.3. Apoptosis assay

For testing the apoptotic potential of new complexes, A549 and LLC1 cells were incubated with these complexes at a concentration of 62.5 μM for 24 h. After incubation, cells were washed and resuspended in ice-cold binding buffer [10 × binding buffer: 0.1 M Hepes/NaOH (pH 7.4), 1.4 M NaCl, 25 mM $CaCl_2$], AnnexinV (BD Pharmingen, San Diego, California, USA) and propidium iodide (Sigma Aldrich) were added. After incubation for 15 min in a dark place, cells were analyzed using a FACS Calibur flow cytometer (BD Biosciences, San Jose, USA). The percentages of viable, early apoptotic, and late apoptotic cells were determined using FlowJo software (Tree Star).

2.6.4. Flow cytometry

A549 and LLC1 cells, grown in culture plates, were exposed to complexes, cisplatin, or medium for 24 h. After fixation and permeabilization, cells were incubated with antibodies specific for Bcl-2, Mcl-1, Noxa, Bax, pAKT, Ki-67, and cyclin D1. The detection of cells expressing Bcl-2, Mcl-1, Noxa, Bax, pAKT, Ki-67, and cyclin D1 was done by a FACSCalibur flow cytometer (BD Biosciences). The data were analyzed using FlowJo software (Tree Star).

2.6.5. Experimental animals

Eight- to ten-week-old C57BL/6 mice of equal weight were selected for the experiments. All experimental animals were housed in standard conditions. All experiments were approved by and conducted in accordance with the Guidelines of the Animal Ethics Committee of the Faculty of Medical Sciences of the University of Kragujevac, Serbia.

2.6.6. Heterotopic model of murine Lewis lung cancer and drug treatment

C57BL/6 mice were injected with 5×10^4 LLC1 cells subcutanously at the back. The mice were randomly separated into four groups 15 days after LLC1 cells were administered, when primary tumors were palpable. Each group contained 5 mice. The first group was treated with complex **2**, the second group with complex **5**, the third group with cisplatin, and the fourth group was treated with saline. Mice received **2**, **5** or cisplatin (5 mg/kg body weight) or saline in six doses, three doses per week, and were sacrificed on the 26th day after injection of tumor cells.

2.6.7. Evaluation of primary Lewis lung cancer volume

The primary heterotopic LLC1 tumor size was morphometrically measured in two dimensions using a caliper. The formula used to determine the tumor volumes (mm^3) is: tumor volume (mm^3) = L (major axis of the tumor) × W(minor axis)^2/2.

2.6.8. Histological analysis

Lung tissue slices were cut into thin sections, immersed in paraffin, fixed in 4% paraformaldehyde, mounted on glass slides, and stained with hematoxylin and eosin. Slides were examined for the existence of metastases using a digital camera-equipped low-power light microscope

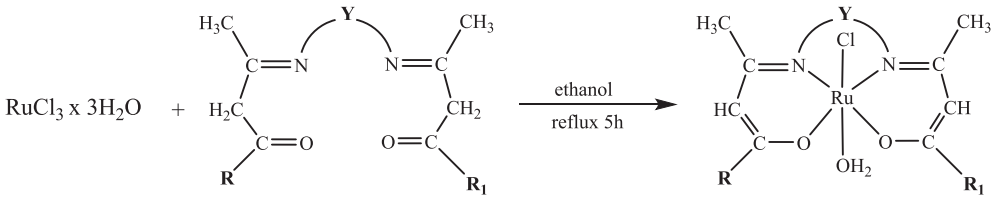

R	R1	Y		
CH_3	CH_3	CH_2CH_2	acacen	(**1**)
Ph	Ph	CH_2CH_2	bzacen	(**2**)
Ph	CH_3	CH_2CH_2	acacbzacen	(**3**)
CH_3	CH_3	CH_2CHCH_3	acacpn	(**4**)
Ph	Ph	CH_2CHCH_3	bzacpn	(**5**)
Ph	CH_3	CH_2CHCH_3	acacbzacpn	(**6**)

Scheme 1. Synthetic route for the preparation of complexes **1–6**.

Table 1
EPR data of the complexes **1–6.**

Complex	g_x	g_y	g_z
1	2.27	2.27	1.83
2	2.25	2.25	1.84
3	2.25	2.25	1.85
4	2.29	2.29	1.81
5	2.24	2.24	1.87
6	2.27	2.27	1.82

Table 2
DNA constants (K_b, K_{sv}) derived for **1–6** from EB (K_{sv} [a]) and Hoechst–DNA fluorescence (K_{sv} [b]).

Complex	K_b [M^{-1}]	K_{sv} [a] [M^{-1}]	K_{sv} [b] [M^{-1}]
1	$(5.8 \pm 0.3) \times 10^4$	$(4.9 \pm 0.2) \times 10^3$	$(4.4 \pm 0.3) \times 10^4$
2	$(8.8 \pm 0.2) \times 10^4$	$(2.1 \pm 0.1) \times 10^4$	$(1.8 \pm 0.3) \times 10^4$
3	$(6.4 \pm 0.2) \times 10^4$	$(5.9 \pm 0.2) \times 10^3$	$(4.0 \pm 0.1) \times 10^4$
4	$(6.1 \pm 0.1) \times 10^4$	$(5.6 \pm 0.1) \times 10^3$	$(4.5 \pm 0.2) \times 10^4$
5	$(8.6 \pm 0.2) \times 10^4$	$(7.8 \pm 0.3) \times 10^3$	$(2.4 \pm 0.2) \times 10^4$
6	$(7.1 \pm 0.1) \times 10^4$	$(7.4 \pm 0.1) \times 10^3$	$(2.6 \pm 0.1) \times 10^4$

(BX51; Olympus).

3. Results and discussion

3.1. Synthesis and characterization

Here, we present a series of new ruthenium compounds with the general formula [Ru(*L*)Cl(H_2O)], where L is tetradentate Schiff base ligand *bis*(acetylacetone)ethylendiimine (acacen, **1**), *bis*(benzoylacetone)ethylendiimine (bzacen, **2**), (acetylacetone) (benzoylaceton) ethylendiimine (acacbzacen, **3**), *bis*(acetylacetone)propylendiimine (acacpn, **4**), *bis*(benzoylacetone) propylendiimine (bzacpn, **5**) or (acetylacetone)(benzoylaceton) propylendiimine (acacbzacpn, **6**). The synthesis procedure for complexes **1–6** is depicted in Scheme 1. The synthesis of neutral Ru(III) complexes **1–6** was performed by reacting $RuCl_3 \cdot 3H_2O$ with the respective tetradentate Schiff base under reflux conditions in moderate yields (%). All complexes were characterized by molar conductometry, elemental analysis, and a variety of spectroscopic techniques, such as EPR, UV–Vis, IR, and ESI-MS spectroscopy.

The infrared spectra of free ligands and corresponding Ru(III) complexes were carefully examined to determine the coordination mode of ligands. Stretching vibrations ν(O—H) in the region between 3445 and 3438 cm^{-1} were observed due to the coordinated water in **1–6** [19]. The IR spectra show the aromatic and aliphatic C—H stretching in the range 3099–2925 cm^{-1} and the strong band assigned to ν(C=C) stretching in the range 1621–1485 cm^{-1} [20]. The strong bands in the range between 1289 and 1285 cm^{-1} were observed in the free Schiff bases due to enolic ν(C—O) stretching vibrations (Fig. S3). These bands of the complexes **1–6** were shifted to the higher wavenumbers in the region between 1325 and 1362 cm^{-1}, demonstrating the coordination of the Ru(III) ion via the enolic oxygen atom (Fig. S4) [21,22]. The ν(CH=N) vibrations of free Schiff bases showed a strong band in the region 1371–1324 cm^{-1}. The coordination of the nitrogen atom of the azomethine group with the Ru (III) ion was confirmed by the shifting of this band to a higher vibration frequency in **1–6** (1447–1435 cm^{-1}) [5]. The electronic absorption spectra of **1–6**, recorded in dimethyl-sulfoxide, showed several absorption bands. Due to the presence of a non-bonding electron on the nitrogen of the azomethine group of the Schiff bases, the absorption bands in the region around 259–274 nm and 313–325 nm were assigned to π–π* and n–π* transitions, respectively (Fig. S5) [23,24]. A moderately intense band in the visible region between 403 and 410 nm was assigned to the ligand-to-metal charge-transfer (LMCT) transition [25]. The absorption spectra of **1–6** are characteristic of the octahedral environment around the Ru(III) ions. The molar conductivity (Λμ) values of **1–6** in 10^{-3} M DMF solution at ambient temperature were 7.0–24.3 μS cm^{-1}, revealing the essential non-electrolytic character of the complexes [26]. Additionally, the electrospray ionization (ESI) mass spectra of **1–6**, obtained in positive mode, are presented in Fig. S6. The loss of one chloride atom for all ruthenium complexes appears to be common under ESI-MS conditions [27–29]. The ESI-MS spectra revealed the presence of a signal arising from the $[Ru(L)(H_2O)]^+$ and $[Ru(L)]^+$ molecular ions. Electron paramagnetic resonance (EPR) spectra of **1–6** obtained in the solid state (X-band, 295 K) show a very broad line (Fig. S7). The spectra strongly suggest the paramagnetic character in the low spin Ru(III) centers in distorted octahedral geometry. By fitting, it was obtained that the spectra are axially symmetrical, i.e., $gx = gy = g\perp > gz = g\|$, indicating orthogonal symmetry elongated along the Z axis (Table 1). The lines in the EPR spectra of **1–6** are identical in nature and position to those in other ruthenium(III) complexes [30].

3.2. DNA binding studies

During the development of metallotherapeutics, some early reports on the action mechanism of ruthenium anticancer compounds suggested that interaction with DNA was responsible for their anticancer activity, similar to cisplatin [31,32]. DNA can act as a ligand either through coordination to the bases or interactions with the sugar phosphate backbone. Furthermore, non-covalent interactions with DNA can involve intercalation, which takes place when a planar, aromatic moiety slides in between two adjacent nucleobases on the same side of the DNA chain,

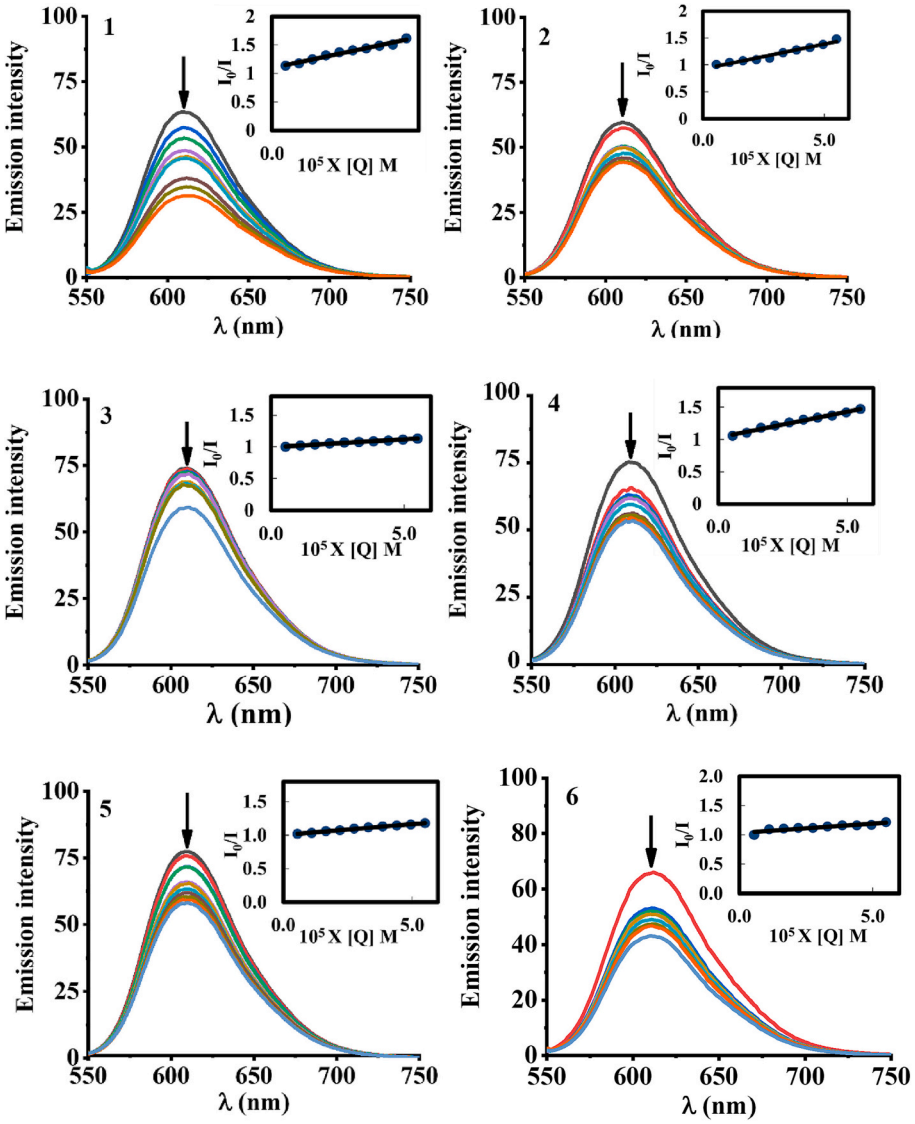

Fig. 2. Emission spectra of EB bound to DNA in the presence of **1–6**. [EB] = 27,5 μM, [DNA] = 28,6 μM; [complex] = 0–55 μM; λex = 527 nm. The arrows depict the change in intensity as complex concentration increases. Insert graphs: Stern-Volmer quenching plots of EB-DNA for **1–6**.

and DNA groove binding via a combination of hydrogen-bonding, electrostatic, and hydrophobic interactions [33]. Keeping this in mind, it is essential to determine the binding constant and type of bonding between a metal complex and DNA. The DNA-binding ability of complexes was followed by changes in the spectra of the selected compounds after the addition of an increasing concentration of CT DNA (Fig. S8). The hyperchromic changes of the UV–Vis spectra indicated that complexes **1–6** bind moderately to CT DNA. The binding constants, K_b, of **1–6**, presented in Table 2, were calculated by the eq. S1, ESI, and the plots (Fig. S9, ESI). The binding constant values followed the order: **2** (bzacen) ≈ **5** (bzacpn) > **6** (acacbzacpn) > **3** (acacbzacen) > **4** (acacpn) > **1** (acacen). Ru complexes **2** (bzacen) and **5** (bzacpn) showed the greatest binding affinity to CT DNA, demonstrating that the presence of the aromatic rings on the tetradentate ligand has an important effect on the increased DNA activity. Additionally, we found that the complexes bearing Schiff base ligands made from propylenediamine (**4**, **5**, and **6**) showed higher binding affinity to DNA than those bearing ethylendiamine (**1**, **2**, and **3**), respectively, implying that the presence of the methyl groups contributes to increased activity. For comparison, new tumor-selective Ru compounds of the general formula $Na[RuCl_2(L^{1-3}\text{-}N,O)_2]$, where $L^{(1-3)}$ refer to deprotonated Schiff bases (HL^1–HL^3) made from alkylamine (propyl- or butylamine) and 5-substituted salicyladehyde with strong activity against MDA-MB-231 cisplatin-resistant breast carcinoma, showed lower DNA-binding affinity with K_b values of order 10^3 compared to complexes **1–6** with K_b values of 10^4 [34].

Competitive ethidium bromide (EB) displacement was carried out to further investigate the DNA-binding affinity between **1 – 6** and CT DNA. The increasing concentrations of **1–6** in the EB–CT DNA adduct solution result in a moderate decrease in the intensity of the band at 612 nm (Fig. 2). The emission quenching data were examined using the Stern–Volmer eq. (S2, ESI), and the calculated values of Stern–Volmer (K_{sv}) were presented in Table 2. The fluorescence intensity of EB-DNA diminished after each addition of the complex, demonstrating competition for DNA binding between the compound and EB. The values of the quenching constants, K^a_{sv}, for the interaction of **1–6** with CT DNA followed the same affinity pattern that we observed for the binding constants, K_b, i.e.: **2** (bzacen) ≈ **5** (bzacpn) > **6** (acacbzacpn) > **3** (acacbzacen) > **4** (acacpn) > **1** (acacen). Considering that the complexes with aromatic ligands (**2** and **5**) showed the most efficient competition in binding to CT DNA with EB, this indicates that the reduced number of aromatic rings or their absence causes lower intercalative properties of the complexes. In the cases of **1** and **4** with non-aromatic units, weak fluorescence quenching and moderate binding constants might suggest

Table 3
BSA constants (K_{sv}, k_q) for the interactions of **1–6** in the absence and presence of Ibuprofen or Eozin Y.

Complex	No site marker		Ibuprofen		Eozin Y	
	K_{sv}	k_q	K_{sv}	k_q	K_{sv}	k_q
1	$(7.7 \pm 0.4) \times 10^3$	7.7×10^{11}	$(1.5 \pm 0.4) \times 10^4$	1.5×10^{12}	$(2.0 \pm 0.2) \times 10^4$	2.0×10^{12}
2	$(6.8 \pm 0.2) \times 10^4$	6.8×10^{12}	$(3.1 \pm 0.2) \times 10^4$	3.1×10^{12}	$(8.9 \pm 0.1) \times 10^3$	8.9×10^{11}
3	$(3.5 \pm 0.1) \times 10^4$	3.5×10^{12}	$(2.8 \pm 0.3) \times 10^4$	2.8×10^{12}	$(2.2 \pm 0.3) \times 10^4$	2.2×10^{12}
4	$(1.6 \pm 0.3) \times 10^4$	1.6×10^{12}	$(1.7 \pm 0.1) \times 10^4$	1.7×10^{12}	$(1.4 \pm 0.1) \times 10^4$	1.4×10^{12}
5	$(7.6 \pm 0.2) \times 10^4$	3.5×10^{12}	$(5.0 \pm 0.2) \times 10^4$	5.0×10^{12}	$(1.2 \pm 0.2) \times 10^4$	1.2×10^{12}
6	$(3.3 \pm 0.1) \times 10^4$	3.3×10^{12}	$(2.6 \pm 0.3) \times 10^4$	2.6×10^{12}	$(3.0 \pm 0.3) \times 10^4$	3.0×10^{12}

the minor groove as the preferred mode of binding. It is worth noting that a number of Ru compounds classified as minor groove binders have shown considerable antitumor activity [35].

Moreover, to gain an improved comprehension of the binding mode of **1–6** to DNA, a competitive binding experiment with 2-(4-hydroxyphenil)-5-[5-(4-methylpipera-zine-1-yl)benzimidazo-2-yl]-benzimidazole (Hoechst 33258) which has a specific mode of binding to the minor grove of CT DNA, was performed. Here, we studied the groove binding manner of **1–6** by measuring the changes in the fluorescence spectra of the Hoechst–DNA adduct with increasing amounts of **1–6** (Fig. S10, ESI). Upon excitation at 346 nm, the displacement of bound Hoechst by **1–6** results in a decrease in the emission intensity of the band at 490 nm. The Stern–Volmer plots I_0/I vs. [Q] (Fig. S10, insert graphs, ESI) were calculated using eq. S2, ESI, and presented in Table 2. The Hoechst-quenching constants, K_{sv}^b, follow the opposite affinity trend as we obsarved for the EB-fluorescence quenching, i.e., **4** (acacpn) ≈ **1** (acacen) > **3** (bzacen) > **6** (bzacpn) > **5** (acacbzacpn) > **2** (acacbzacen). The

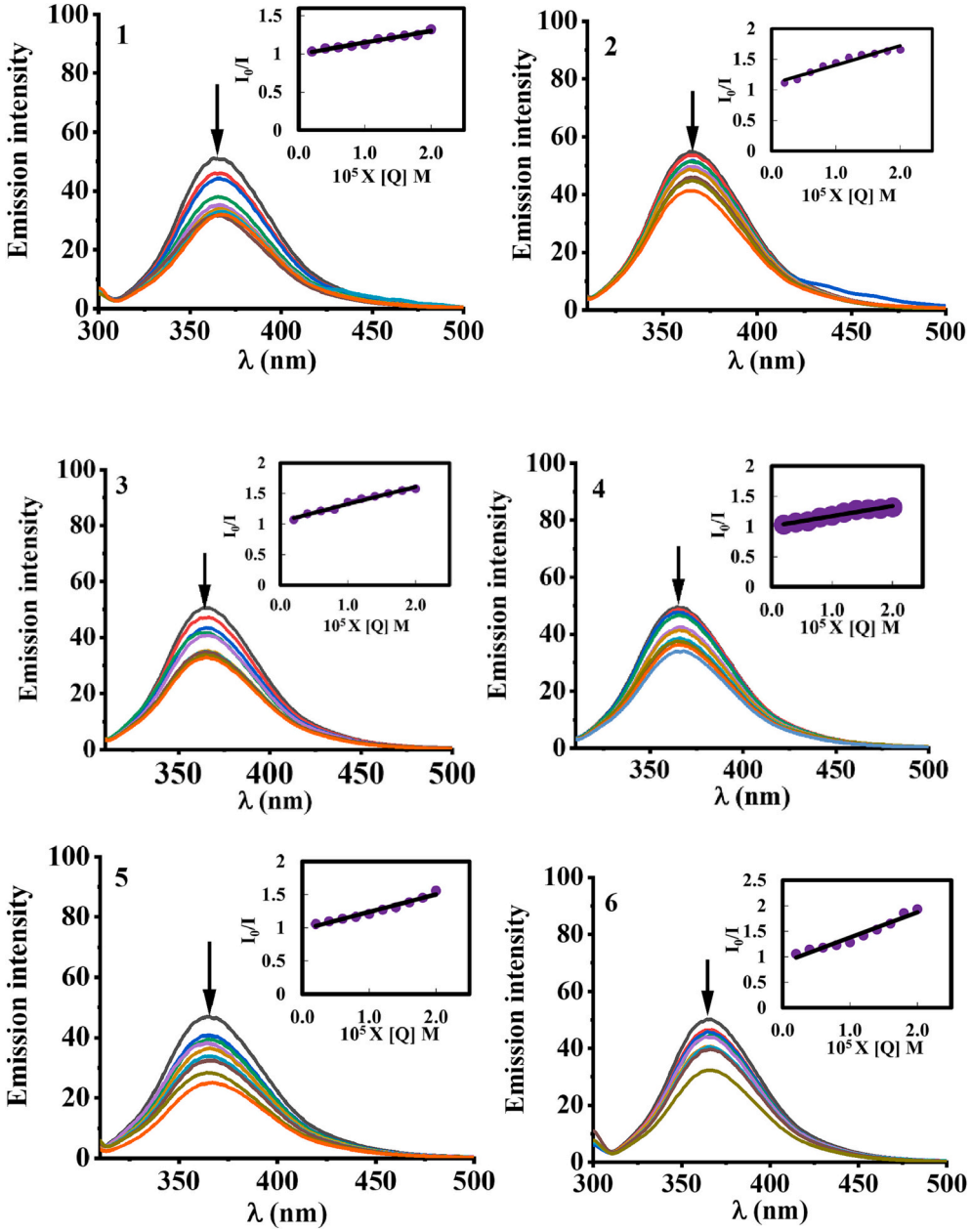

Fig. 3. BSA-Ibuprofen emission spectra in the presence of **1–6**. The arrow depicts the changes in fluorescence intensity as the concentration of complexes increases. Insert graph: BSA-Ibuprofen Stern-Volmer quenching plot for **1–6**.

Table 4
Thermodynamic parameters for the most stable conformations of **1–6** in different DNA conformations obtained after molecular docking simulation. (ΔG_{bind} free energy binding, ΔG_{total} final total internal energy, K_i constant of inhibition, ΔG_{tor} torsional free energy, ΔG_{elec} electrostatic energy and $\Delta G_{vdw+hbond+desolv}$ is the sum of dispersion and repulsion (ΔG_{vdw}), ΔG_{unb} unbound system's energy, desolvation (ΔG_{desolv}) and hydrogen bond (ΔG_{hbond}) energy, kcal mol^{-1}).

Conformations	ΔG_{bind}	K_i (μM)	ΔG_{inter}	$\Delta G_{vdw+hbond+desolv}$	ΔG_{elec}	ΔG_{total}	ΔG_{tor}	ΔG_{unb}
DNA (**1Z3F**) – **1**	−5.29	133.26	−5.56	−5.37	−0.19	−0.45	0.27	−0.45
DNA (**1BNA**) – **1**	−6.94	8.12	−7.22	−6.97	−0.24	−0.22	0.27	−0.22
DNA (**1Z3F**) – **2**	−9.81	0.65	−10.63	−10.45	−0.18	−1.21	0.82	−1.21
DNA (**1BNA**) – **2**	−7.80	1.90	−8.63	−8.57	−0.06	−1.08	0.82	−1.08
DNA (**1Z3F**) – **3**	−8.50	0.59	−9.05	−8.87	−0.18	−0.84	0.55	−0.84
DNA (**1BNA**) – **3**	−8.05	1.26	−8.60	−8.28	−0.32	−0.53	0.55	−0.53
DNA (**1Z3F**) – **4**	−5.30	130.39	−5.57	−5.54	−0.04	−0.43	0.27	−0.43
DNA (**1BNA**) – **4**	−7.60	6.67	−7.34	−7.09	−0.25	−0.22	0.27	−0.22
DNA (**1Z3F**) – **5**	−9.79	66.73	−10.61	−10.43	−0.19	−1.18	0.82	−1.18
DNA (**1BNA**) – **5**	−7.52	3.09	−8.34	−8.13	−0.03	−1.04	0.82	−1.04
DNA (**1Z3F**) – **6**	−8.51	0.57	−9.06	−8.88	−0.18	−0.87	0.55	−0.87
DNA (**1BNA**) – **6**	−8.04	1.28	−8.59	−8.27	−0.32	−0.54	0.55	−0.54

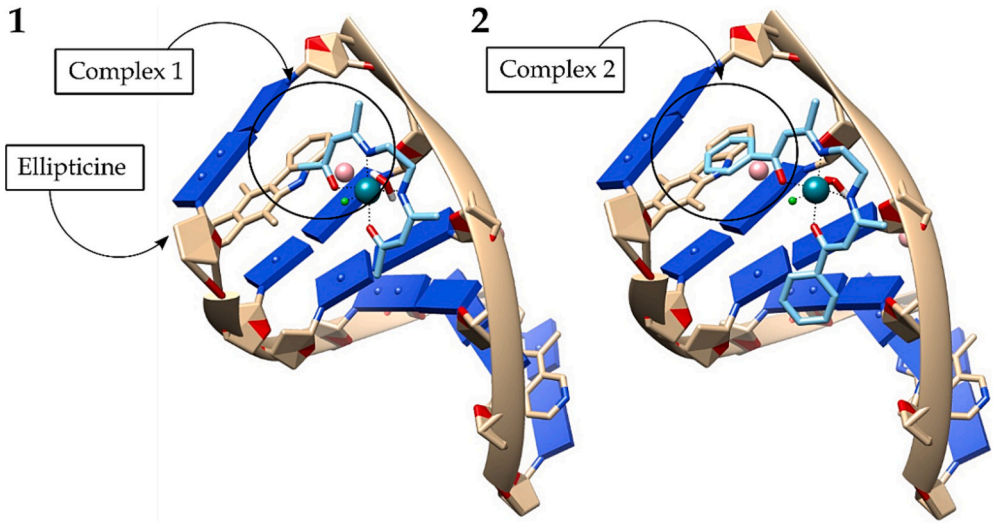

Fig. 4. Superposition of the most favorable binding mode of **1** and **2** with ellipticine in the hexanucleotide $d(CGATCG)_2$ (PDB code: 1Z3F). Complexes **1** and **2** are represented as blue sticks (carbon atoms), while ellipticine is represented as yellow sticks (carbon atoms). The sugar-phosphate backbones of the two complementary chains are shown as spirally twisted yellow bands, while the nucleobases are represented in blue. Different colors on the sticks indicate different atoms: nitrogen-blue, oxygen-red, chlorine-green, and ruthenium ion–sphere of dark green color. (For interpretation of the references to color in this figure legend, the reader is referred to the web version of this article.)

calculated values clearly demonstrated that complexes with non-aromatic ligands (**1** and **4**) had the highest ability to displace Hoechst molecules bound to DNA, suggesting the minor groove as the preferred binding mode.

In the absence of more rigorous data like crystallographic structure, hydrodynamic viscosity measurement, which is very sensitive to length change, is regarded as the most crucial test for binding mode in solution. Viscosity measurements were performed to better understand the DNA binding mode of **1–6**. Electrostatic interaction causes no change in viscosity, however, partial intercalation can cause a decrease in the relative viscosity of DNA [36]. Furthermore, classical intercalators result in lengthening the DNA helix, which leads to an increase in DNA viscosity. The relative DNA viscosity changes in the presence of increasing concentrations of **1–6** showed the same trend as EB quenching measurements. Complexes with the aromatic rings (**2**, **3**, **5**, and **6**) showed a greater increase in DNA viscosity compared to those with methyl groups (**1** and **4**), respectively. Moreover, **1** and **4** caused a decrease in the DNA relative viscosity (Fig. S11).

3.3. BSA binding studies

Knowing that serum proteins play an important role in drug transport and deactivation, we studied the interactions of **1–6** with the major metal-transporting serum protein albumin by florescence spectroscopy. Bovine serum albumin (BSA) is the most examined serum albumin, owing to its structural similarity to human serum albumin. The interactions of ruthenium complexes with serum albumins have been thoroughly investigated to examine their anticancer activity, as binding to an appropriately stable protein-drug complex has a significant impact on drug distribution and efficacy. Addition of **1–6** to a BSA solution (up to r values of 20 μM, Fig. S12) results in weak to moderate quenching of BSA fluorescence at $\lambda = 352$ nm. The linear decrease in BSA fluorescence with increasing quencher concentration followed the Stern–Volmer equation (Fig. S13). The emission quenching data from the BSA experiments were analyzed according to the double logarithmic eq. (S5). The K_{sv} and K_b values of order 10^3 and 10^4 M^{-1} (Table 3), respectively, revealed weak to moderate interactions between BSA and **1–6** with the number of binding sites near 1 (the Scatchard plots are presented in Fig. S14, ESI) [37]. Furthermore, the fluorescence maximum was slightly red shifted (Fig. S12, ESI), implying the formation of ruthenated-protein adducts, which affected the polarity of the microenvironment near tryptophan. The observed BSA-binding affinity followed the same trend as for the DNA interactions: **2** > **5** > **3** > **6** > **4** > **1**. Complexes **2** (bzacen) and **5** (bzacpn) with two aromatic rings showed the highest BSA-activity, suggesting that the presence of the aromatic ring on the tetradentate Schiff base ligand has a great influence on the increased BSA activity.

Fluorescence titration methods with eosin Y, as a marker for site I of subdomain IIA, and ibuprofen, as a marker for site II of subdomain IIIA, were utilized to obtain deeper insight into the binding location on the BSA molecule. BSA and the markers were added in equimolar concentrations (2 μM), whereas solutions of **1–6** were added at increasing

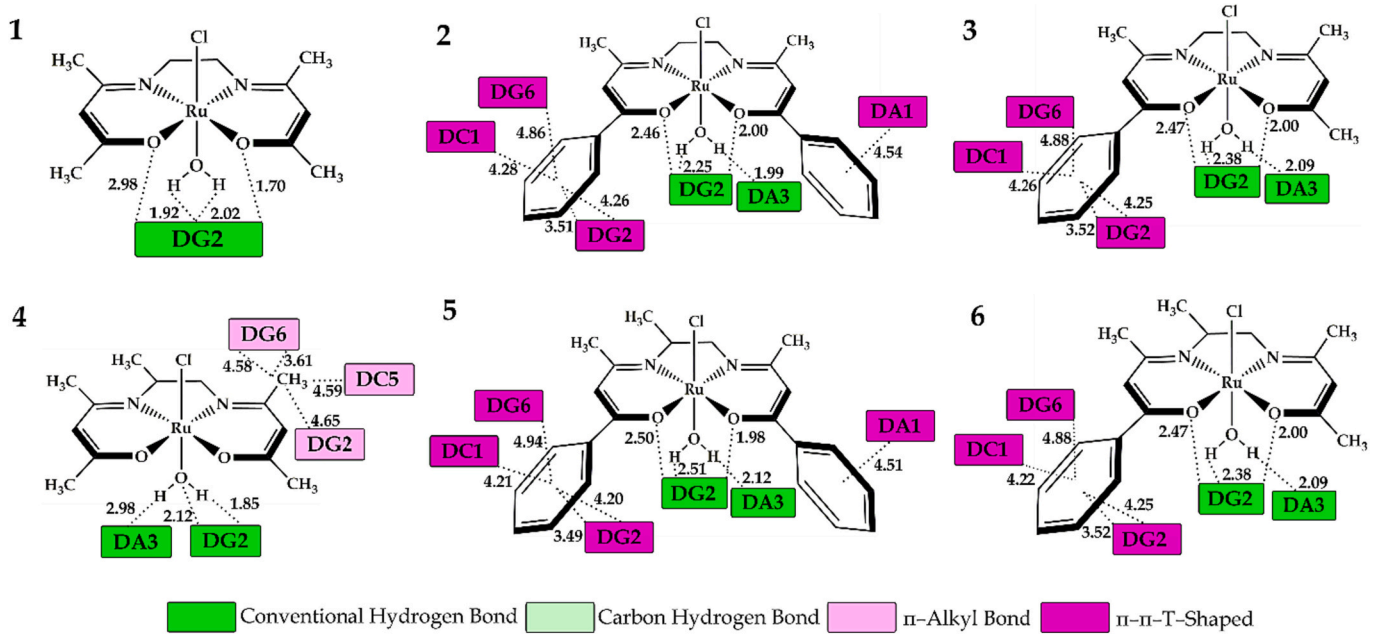

Fig. 5. 2D representation of interactions between complexes **1–6** and nucleobase of hexanucleotide d(CGATCG)$_2$ (PDB code: 1Z3F) with interatomic distance obtained after molecular docking simulation (DC = deoxycytidine; DA = deoxyadenosine; DT = deoxythymidine; DG = deoxyguanosine). Different colors indicate different types of interactions (legend).

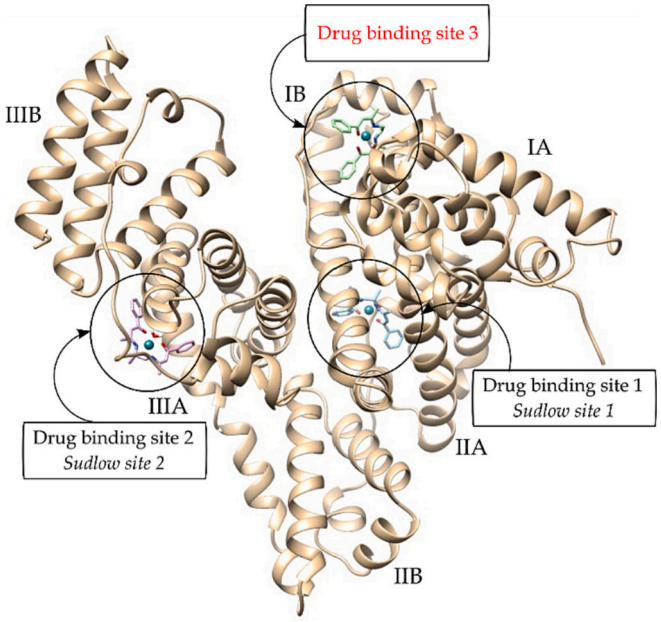

Fig. 6. 3D representation of the best docking position of complex **2** at three different active sites (active site I, II, III) of Bovine Serum Albumin (chain A) (PDB code: 4F5S).

concentrations (up to a ratio of 20 μM). The excitation wavelength for the specific change in BSA fluorescence was 295 nm, with an emission range of 300–500 nm (Fig. 3). The BSA–eosin Y (Fig. S16) and BSA–ibuprofen adducts (Fig. 3), show intense emission, and their displacement by **1–6** from the protein's binding site is accompanied by a moderate decrease in emission intensity. The fluorescence data were evaluated according to the Stern–Volmer and Scatchard eqs. (S3-S5) and plots (Fig. s S16 and 3 Stern- Volmer plots of BSA-EosinY and BSA-Iboprufen, insert graphs, respectively; Fig. s S15 and S17 Scatchard plots of BSA-Iboprufen and BSA-EosinY, respectively). The Stern–Volmer (K_{sv}), bimolecular quenching (k_q) and binding constants (K_b) for the interactions of **1–6** with BSA in the absence and presence of site markers, are depicted in Table 3. The obtained results demonstrated that the studied complexes bind to IIA and IIIA sites with moderate affinity ($K_b = 10^4$ M^{-1}) without preference for any protein binding site. Similar observations were reported for other Ru(III) complexes with Schiff base chelates [38].

3.4. Molecular docking

3.4.1. Molecular docking investigations with DNA

A molecular docking investigation was carried out to obtain a comprehensive description of the interactions between the newly synthesized compounds, **1–6**, and the selected DNA conformations: **1BNA** and **1Z3F**. The dodecameric structure **1BNA** comprises a sequence of d(CGCGAATTCGCG)$_2$. The molecular docking simulation with **1BNA** conformation mimics the canonical mode of interaction of the complexes with the DNA molecule and is parallel to the experimentally confirmed Stern–Volmer constants (K^b_{sv}) obtained from the Hoechst–DNA fluorescence experiment. The second conformation represents the hexanucleotide d(CGATCG)$_2$ with a very powerful anticancer agent – ellipticine, with RSCB PDB code **1Z3F**. The simulation utilizes this conformation potential intercalation and parallels Stern–Volmer constants (K^a_{sv}) obtained from EB–DNA fluorescence experiment.

The optimized geometries of **1–6** used in the molecular docking simulation are presented in Fig. S18. The obtained results for interactions between the investigated compounds and the **1BNA** and **1Z3F** conformations are shown in Table 4. More negative ΔG_{bind} values and lower K_i values indicate that the newly synthesized Ru complexes have a higher DNA–binding affinity. Close energy values suggest that investigated compounds exhibit binding mode competition toward the **1BNA** and **1Z3F** conformations. Based on refined energy differences, it is possible to determine which is the preferential (non-covalent) mode of binding to the DNA helix. The analysis of ΔG_{bind} and K_i values indicates that the complexes that contain aromatic rings **2, 3, 5,** and **6**, exhibit a greater affinity to bind to the intercalation site of the **1Z3F** conformation. The obtained results are consistent with the EB-fluorescence quenching (K^a_{sv}) constants that have been determined through

Table 5
Thermodynamic parameters for the most stable conformations of Ru complexes **1–6** in the different active sites of **BSA** protein obtained after molecular docking simulation. (K_i constant of inhibition, ΔG_{bind} free energy binding, ΔG_{total} final total internal energy, ΔG_{unb} unbound system's energy, ΔG_{tor} torsional free energy, ΔG_{elec} electrostatic energy and $\Delta G_{vdw+hbond+desolv}$ is the sum of dispersion and repulsion (ΔG_{vdw}), desolvation (ΔG_{desolv}) and hydrogen bond (ΔG_{hbond}) energy, kcal mol^{-1}).

Conformations	ΔG_{bind}	K_i (μM)	ΔG_{inter}	$\Delta G_{vdw+hbond+desolv}$	ΔG_{elec}	ΔG_{total}	ΔG_{tor}	ΔG_{unb}
BSA-1-I	−5.49	94.70	−5.76	−5.65	−0.11	−0.46	0.27	−0.46
BSA-1-II	−5.61	77.04	−5.89	−5.90	0.01	−0.45	0.27	−0.45
BSA-1-III	−6.47	18.24	−6.74	−6.61	−0.13	−0.45	0.27	−0.45
BSA-2-I	−6.02	38.39	−6.85	−6.76	−0.09	−1.01	0.82	−1.01
BSA-2-II	−7.87	1.71	−8.69	−8.53	−0.16	−0.93	0.82	−0.93
BSA-2-III	−8.26	0.87	−9.08	−9.15	0.08	−1.19	0.82	−1.19
BSA-3-I	−6.33	22.96	−6.88	−6.65	−0.23	−0.71	0.55	−0.71
BSA-3-II	−6.75	11.32	−7.30	−7.19	−0.11	−0.64	0.55	−0.64
BSA-3-III	−7.78	1.97	−8.33	−8.42	0.08	−0.84	0.55	−0.84
BSA-4-I	−5.97	42.09	−6.24	−6.13	−0.11	−0.44	0.27	−0.44
BSA-4-II	−5.79	56.56	−6.07	−6.05	−0.02	−0.28	0.27	−0.28
BSA-4-III	−6.76	11.09	−7.03	−6.92	−0.12	−0.44	0.27	−0.44
BSA-5-I	−5.47	97.08	−6.30	−6.16	−0.14	−1.19	0.82	−1.19
BSA-5-II	−7.09	6.36	−7.91	−7.84	−0.08	−1.19	0.82	−1.19
BSA-5-III	−8.25	0.90	−9.07	−9.14	0.07	−1.17	0.82	−1.17
BSA-6-I	−6.61	14.17	−7.16	−6.94	−0.23	−0.74	0.55	−0.74
BSA-6-II	−6.79	10.57	−7.34	−7.24	−0.11	−0.65	0.55	−0.65
BSA-6-III	−7.83	1.82	−8.38	−8.44	0.06	−0.85	0.55	−0.85

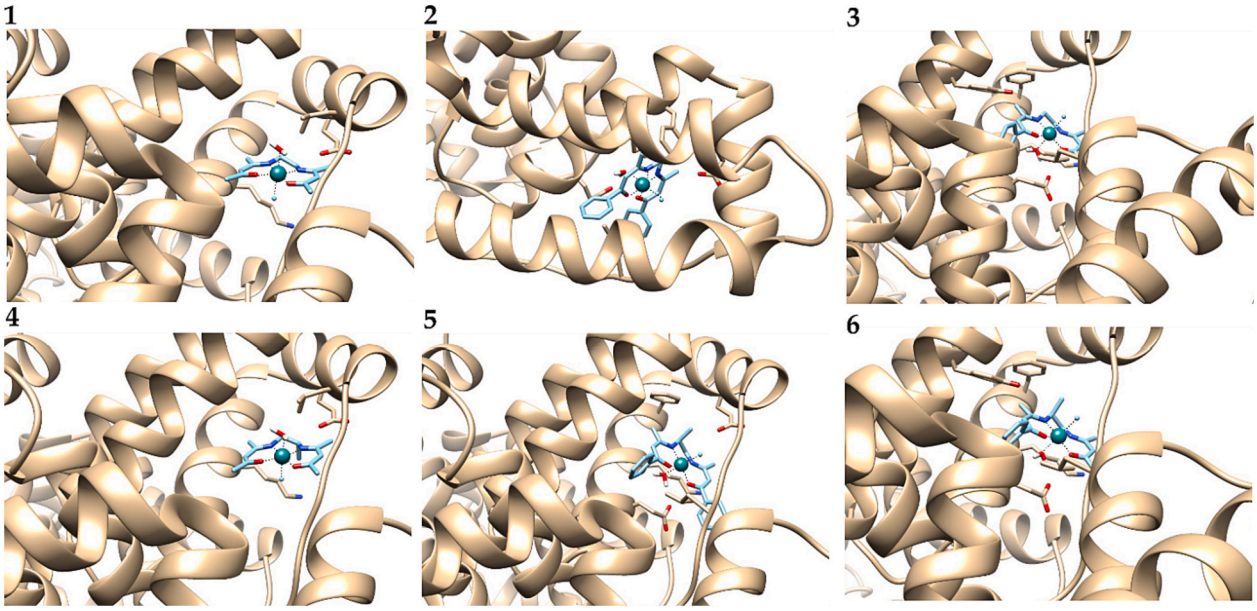

Fig. 7. The most favorable docking position of **1–6** in subdomain IB (active site III) of Bovine Serum Albumin (BSA) (PDB code: 4F5S). Complexes **1–6** are represented as blue sticks (carbon atoms). Different colors on the sticks indicate different atoms: nitrogen-blue, oxygen-red, chlorine-green, and ruthenium ion–sphere of dark green color. For clarity, the remainder of the protein structure has been omitted. (For interpretation of the references to color in this figure legend, the reader is referred to the web version of this article.)

experimentation. A molecular docking study revealed that the complexes with methyl groups, **1** and **4**, have a greater affinity for the **1BNA** conformation, indicating that these compounds bind via a minor groove. The results obtained for these two complexes are consistent with the experimental values of Hoechst-quenching constants (K_{sv}^{b}), which suggest a minor groove as the preferred mode of binding. Decreasing the number of aromatic rings decreases the affinity toward the intercalation site, which is in agreement with the order of decreasing DNA activity according to the **1Z3F** structure: **2 > 5 > 6 > 3 > 4 > 1**. This is an expected result because as the surface area and/or hydrophobicity of the complex increase, so does its DNA binding affinity.

Fig. 4 explains the greater affinity of the complexes obtained with an aromatic ring for the intercalation site of the **1Z3F** conformation. Namely, aromatic rings of **2, 3, 5**, and **6** interact with nucleobases, whereby one of the aromatic rings intercalates into the position of the aromatic ring of ellipticine. On the other hand, the absence of aromatic rings limits the ability of **1** and **4** to intercalate into **1Z3F**. Both complexes preferred to approach the **1BNA** via the minor groove without disrupting its double helix (Fig. s S19 and S21).

Figs 5 and S18 depict the 2D depiction of the interactions between the Ru complexes and the nucleobases of the **1Z3F** and **1BNA** conformations. It was observed that conventional hydrogen bonds stabilized the investigated complexes at the intercalation site of the DNA hexanucleotide (Fig. 5). In general, **DG2** establishes a bifurcated conventional hydrogen bond with the polarized oxygen atoms of the Ru complexes through the $–NH_2$ groups of the purine ring (>1.70 Å). In addition, the coordinated H_2O molecule forms hydrogen bonds with the N and O heteroatoms of two successive nucleobases: **DG2** (>1.85 Å) and **DA3** (>1.19 Å) purine rings (Fig. 5). Hydrophobic interactions significantly contribute to the stability of the investigated compounds at the

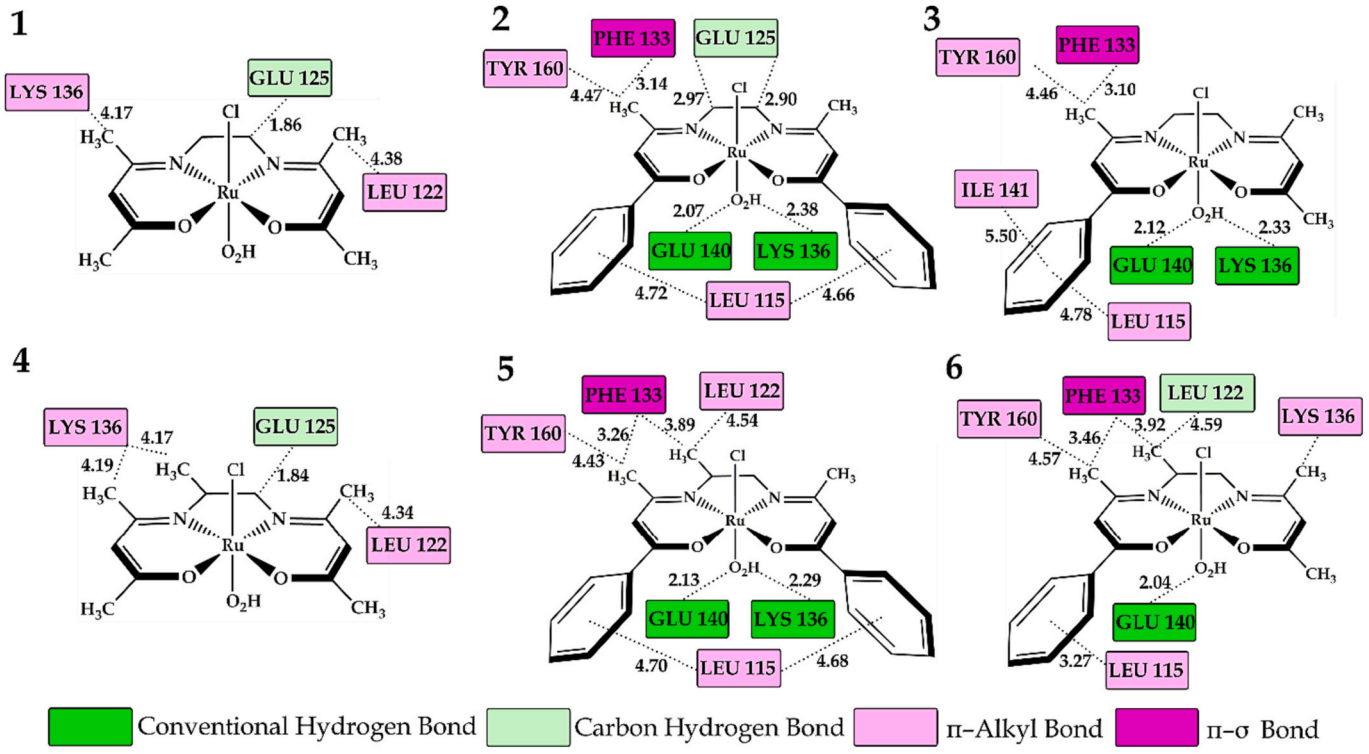

Fig. 8. 2D representation of interactions between complexes **1–6** and amino acid residues in subdomain IB (active site III) of Bovine Serum Albumin (BSA) (PDB code: 4F5S) with interatomic distance obtained after molecular docking. Different colors indicate different types of interactions (legend).

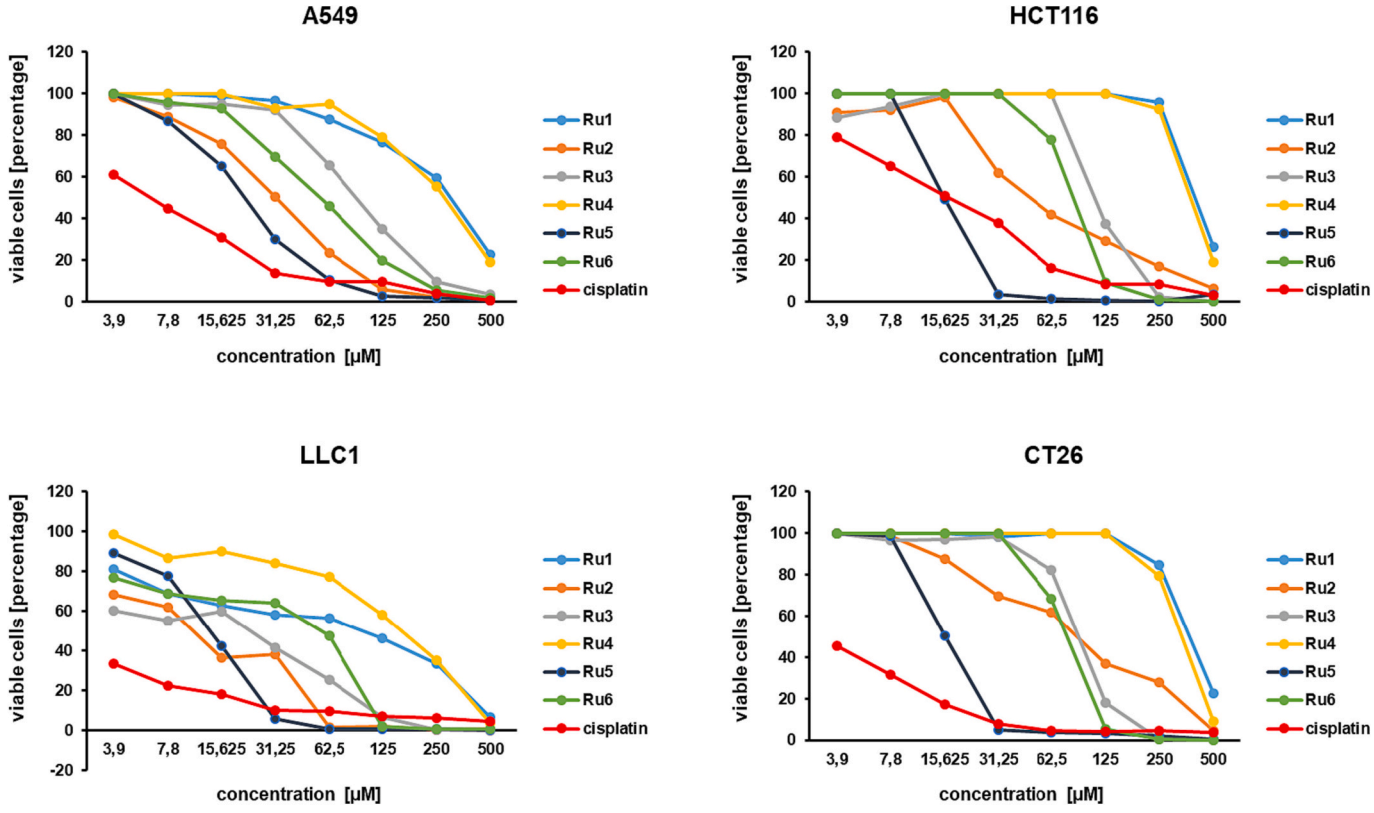

Fig. 9. Cytotoxicity of **1–6** on A549, LLC1, HCT116, and CT26 cell lines after 72 h of exposure (measured by MTT test).

Table 6
IC50 values for cytotoxic activity of **1–6** and cisplatin determined by the MTT assay.

Cell line	IC_{50} ± SD (μg/mL)			
	A549	HCT116	LLC1	CT26
1	284.1 ± 51.2	374.1 ± 82.3	69.0 ± 14.1	486.5 ± 112.1
2	33.5 ± 7.3	48.9 ± 9.2	13.6 ± 3.5	108.5 ± 21.5
3	113.4 ± 19.1	86.2 ± 13.5	23.5 ± 4.1	82.6 ± 17.1
4	369.6 ± 74.2	457.6 ± 96.7	149.0 ± 32.7	704.6 ± 195.2
5	20.9 ± 4.8	16.9 ± 4.0	9.3 ± 2.9	17.9 ± 4.7
6	73.8 ± 9.8	113.9 ± 19.2	57.5 ± 9.9	107.1 ± 23.2
cisplatin	5.6 ± 1.2	15.4 ± 4.3	1.6 ± 0.8	3.7 ± 1.2

Table 7
Selectivity index of **1–6** and cisplatin in A549 and HCT116 cell lines. The selectivity index was determined as fraction of the IC50 for MRC-5 and A549 or HCT116 cells.

Selectivity index		
	A549	**HCT116**
1	1.13	0.86
2	1.75	1.20
3	0.90	1.18
4	1.16	0.94
5	0.60	0.75
6	1.11	0.72
cisplatin	3.82	1.38

intercalation site **1Z3F**. Additionally, the investigated compounds are stabilized at the intercalation site by π–π interactions that are established between the aromatic rings of compounds **2, 3, 5,** and **6** and the nucleobases **DG2**, **DC1**, and **DG6**. The ellipticine placed in the intercalation site of the **1Z3F** conformation is stabilized by π-π interactions with the nucleobases mentioned.

On the other hand, conventional hydrogen bonds have a dominant effect on the stabilization of **1–6** in the **1BNA** conformation. As shown in Fig. S20, complexes **1** and **4** are in the vicinity of the cytosine pairs **DC21** (>1.89 Å) and **DC22** (>1.89 Å) with which they form a conventional hydrogen bond. Successive nucleobases **DG4** and **DA5** via –NH– groups form hydrogen bonds with polarized oxygen atoms of **1** and **4**. Carbon-hydrogen bonds are formed between the chlorine atoms of **1** (3.29 Å) and **4** (3.29 Å) and the carbon atom of the nucleobase **DA6**. This interaction is of minor relevance for the overall stabilization of the DNA-complex structure. A reduced number of hydrophobic interactions can be observed in complexes containing aromatic rings. A hydrophobic π–π contact occurs between the aromatic pyrimidine ring of **DC21** and the aromatic rings of **2** (5.35 Å) and **4** (5.38 Å).

3.4.2. *Molecular docking studies with BSA*

A molecular docking investigation was conducted to predict the binding sites and binding affinity of the newly synthesized complexes with bovine serum albumin (**BSA**). **BSA** consists of 583 amino acids on a single polypeptide chain with three clearly defined domains: I (amino acid residues 1–195), II (amino acid residues 196–383), and III (amino acid residues 384–583), with subdomains A and B within each domain [39,40]. Hydrophobic pockets in subdomains IIA and IIIA, through which the majority of drugs are transported, are classified as active sites I (Sudlow site I) and II (Sudlow site II). In recent decades, a third *D*-shaped hydrophobic pocket for drug binding within subdomain IB (active site III) has been discovered [41]. To obtain a comprehensive understanding of the mechanism of interaction between the most stable conformation of Ru complexes and BSA, a molecular docking study was conducted for all three active sites of **BSA** (Fig. 6).

Small differences in the estimated thermodynamic parameters suggest that the investigated compounds exhibit affinity for all active sites of the **BSA** protein. And in this case, subtle energy differences define the dominant active binding site. The significant parameters obtained from the molecular docking analysis are presented in Table 5. Based on the more negative ΔG_{bind} and low K_i values, it can be concluded that all newly synthesized compounds exhibit the highest binding affinity for

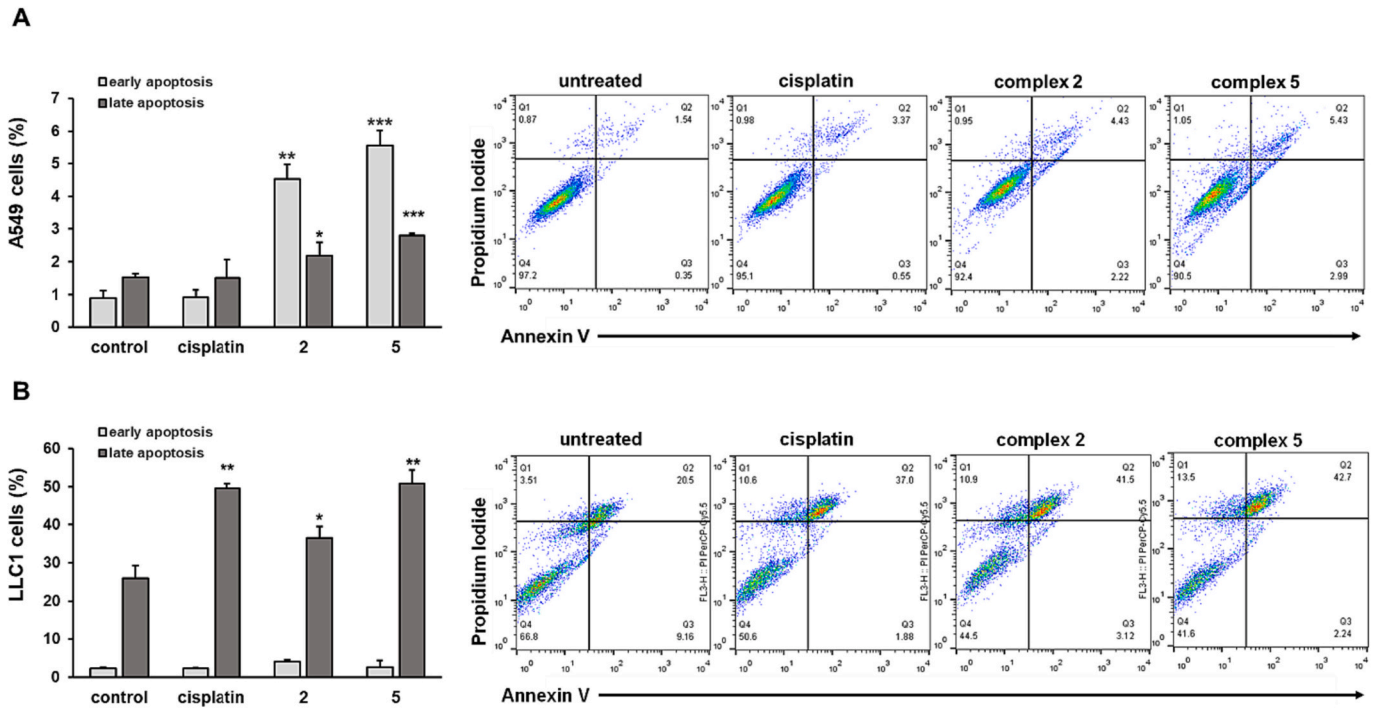

Fig. 10. Ruthenium(III) complexes exhibit a strong apoptotic effect on murine Lewis lung carcinoma cells. Apoptosis of untreated and A549 (A) and LLC1 (B) cells treated for 24 h with cisplatin and complexes **2** and **5,** at a dose of 62.5 μM double stained with Annexin V/PI, was analyzed by flow cytometry. Data are presented as mean + SD, from three independent experiments, $*p < 0.05$ indicate significant difference. Representative dot plots show the populations of viable (AnnV- PI-), early apoptotic (AnnV+ PI-), late apoptotic (AnnV+ PI+) and necrotic (AnnV- PI+) A549 (A right panel) and LLC1 (B right panel) cells.

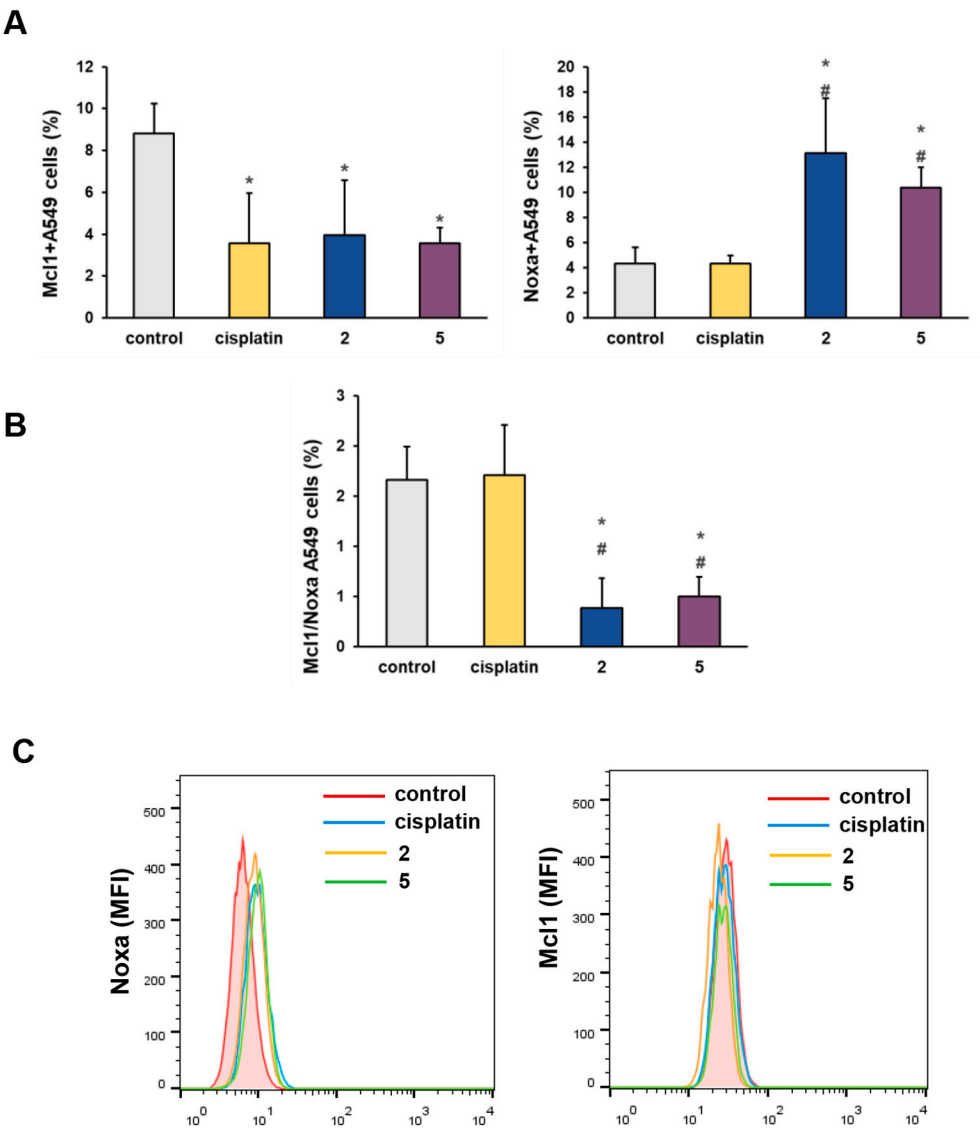

Fig. 11. Ruthenium(III) complexes **2** and **5** change the Mcl1 to Noxa ratio in A549 cells. The graphs show the mean + SD from three independent experiments for (A) the percentage of Noxa and Mcl1 positive A549 cells and (B) the Mcl1 to Noxa ratio. The statistical significance was determined by the Student's *t*-test; * $p < 0.05$ indicates the difference in the percentage of A549 cells treated with **2** and **5**, and untreated cells, # $p < 0.05$ indicates the difference in the percentage of A549 cells treated with **2** and **5**, and cisplatin-treated cells. (C) Representative histogram of Noxa and Mcl1 expression (mean fluorescence intensity) in A549 cells.

active site III. The obtained results are consistent with the available literature data that demonstrate the predominance of large porphyrin ruthenium complexes in binding affinity to active site III [42]. The order of binding activity/affinity decreases in the following order: **2 > 5 > 6 > 3 > 4 > 1**. The order of the activities is correlated to the experimentally determined Stern-Volmer constants values (K_{sv}). As anticipated, compounds with the most aromatic rings, **2** and **5,** have the highest affinity for hydrophobic active sites, whereas compounds without aromatic rings, **1** and **4**, have the lowest binding affinity.

The 3D representation of the most stable conformations of **1–6** in active sites I, II, and III is displayed in Fig. 7, S22, and S24, respectively. The presented structures give the geometries of the most stable docked conformations of **1–6** located in the hydrophobic pockets of the **BSA** protein.

To acquire a thorough understanding of the binding mechanism of the investigated compounds for **BSA**, it is necessary to discuss the interactions between the investigated compounds and amino acid residues. Analyzing the interactions between compounds **1–6** in the active site I reveal that electrostatic interactions dominate the overall stabilization (Fig. S23). Interestingly, differently positioned amino acid residues of arginine: ARG 194, ARG 198, and ARG 217, dominantly participate in the formation of electrostatic (attractive charges and π–anion) and conventional hydrogen bonds with polar atoms of the Ru complexes. On the other hand, in active site II, Ru complexes are dominantly stabilized by a sequence of hydrophobic interactions (π–Alkyl) especially with successive amino acid residues: VAL 408–ARG 409, ARG 412–LYS 413 (Fig. S25).

Finally, special attention is paid to the description of interactions between the compounds under investigation and active site III (Fig. 8).

The partially negative oxygen atom of the amino acid residue GLU 125 forms a carbon-hydrogen bond with the hydrogen atom of the –CH– group of **1** (1.86 Å) and **4** (1.84 Å). These compounds are additionally stabilized by hydrophobic π-alkyl contacts with the amino acids LEU 122 and LYS 136. On the other hand, amino acid residues LYS 136 and GLU 140 via partially negative oxygen atoms form bifurcated conventional hydrogen bonds with the coordinated water molecule of **2, 4, 5**, and **6**. The amino acid residues LEU 115, LEU 122, and TYR160 are involved in the formation of π-alkyl interactions between of π-alkyl contacts with aromatic rings and methyl groups of **2**, **4**, **5**, and **6**. Additionally, an interaction between the aromatic ring of PHE 133 and the σ orbital of the –CH– groups of the investigated compounds is formed (π–σ contact).

3.5. *In vitro studies*

Ruthenium based complexes are reported to exert significant, even higher potency anticancer activities in colorectal carcinoma compared

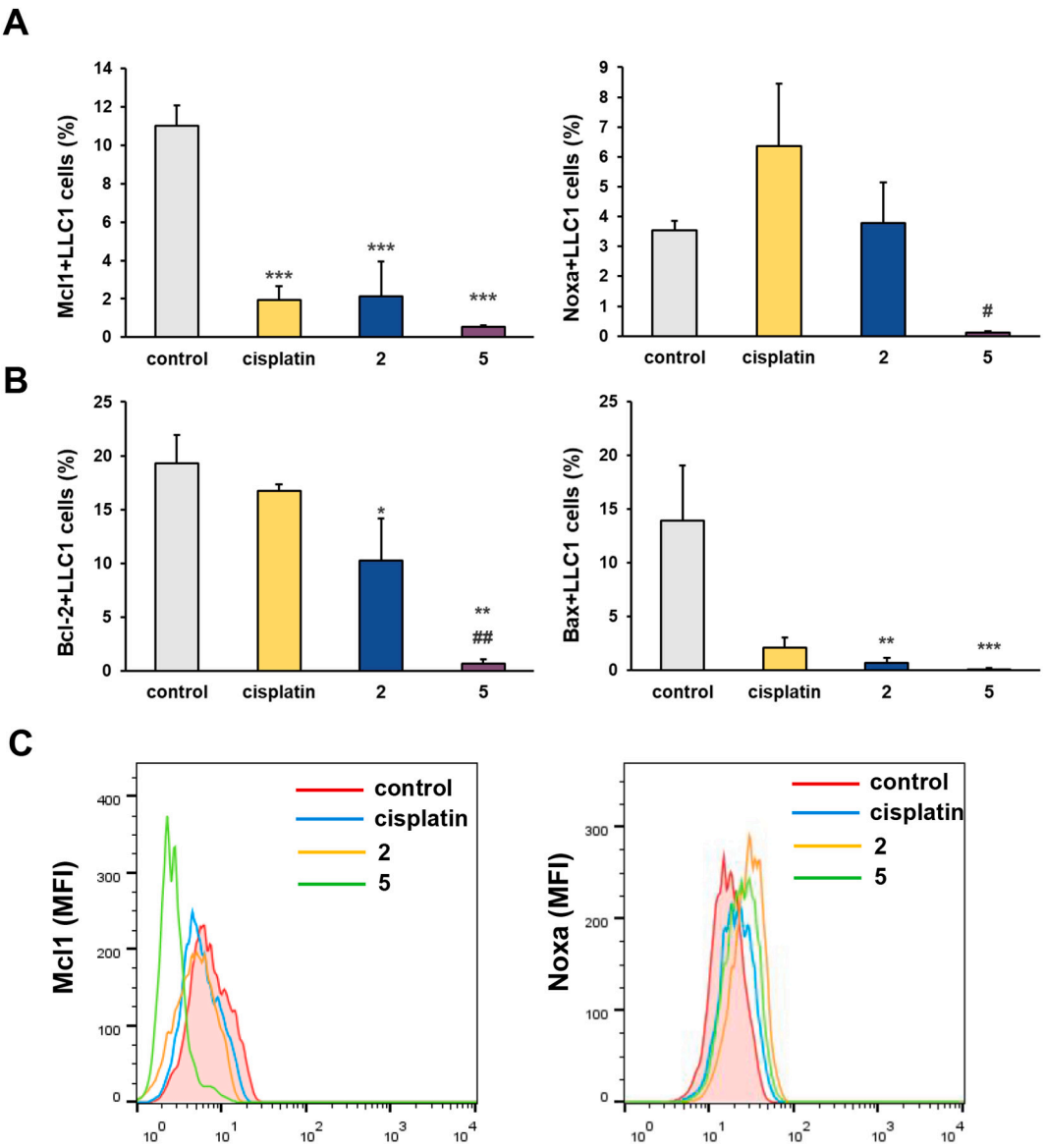

Fig. 12. Complexes **2** and **5** decrease the percentage of LLC1 that express anti- and pro- apoptotic molecules. The graphs show the mean + SD for three independent experiments for the percentages of (A) Noxa and Mcl1, and (B) Bcl-2, and Bax expressing LLC1 cells. The statistical significance was determined by the Student's t-test; * $p < 0.05$, ** $p < 0.01$, and *** $p < 0.005$ indicate the difference in the percentage of LLC1 cells treated with **2** and **5**, and untreated cells, # $p < 0.05$ and ## $p < 0.01$ indicate the difference in the percentage of LLC1 cells Ru- and cisplatin-treated cells. (C) Representative histogram of Noxa and Mcl1 expression (mean fluorescence intensity) in LLC1 cells.

to standard platinum based drugs, by regulating different cell signaling pathways that control cell growth, proliferation, and migration. [43] We have also shown significant in vitro anticancer activity of ruthenium complexes against human and murine colorectal cancer cells [44,45]. Ruthenium complexes are also reported as good candidates for the treatment of lung tumors [46].

Here, we used an MTT assay to evaluate the cytotoxic activity of **1–6** on lung and colorectal carcinoma. All tested compounds exhibited dose-dependent cytotoxicity against A549 and LLC1 cells, but lower compared to cisplatin (Fig. 9). The strongest cytotoxic effects toward A549 and LLC1 had **2** and **5**, especially in medium doses of 31.25 and 62.5 μM when their cytotoxic activity was comparable to cisplatin. The lowest antitumor activity, evaluated by MTT assay, showed **1** and **4**. Complexes **2, 3, 5,** and **6** exerted dose-dependent, moderate antitumor activity on clorectal cancer cells HCT116 and CT26. Furthermore, **1** and **4** reduced the viability of colorectal cancer cells only when the highest concentration (500 μM) was used. The most cytotoxic agent against colorectal cancer cell lines was **5**, especially in medium doses when its activity toward HCT116 cells was better compared to cisplatin.

It is evident that all complexes exert better cytotoxic activity toward lung cancer than toward colorectal cancer cell lines (Table 6). Furthermore, analysis of the IC50 values calculated for the tested Ru(III)-complexes and cisplatin shows that **5** exhibits the strongest antitumor effect on all explored cell lines. Lower but also considerable cytotoxic activity has **2**, while **4** shows the weakest cytotoxic effect, followed by **1**.

In order to explore the selectivity of **1–6** for cancer cell lines, we tested their cytotoxicity toward normal fibroblasts, calculated IC50 values and selectivity index, which is the most commonly reported as a simple ratio of IC50 calculated for healthy and cancer cells [47]. Analysis of the selectivity index revealed that all tested complexes had a lower selectivity index compared to cisplatin (Table 7). Complex **5,** which exhibited the greatest cytotoxicity on all tested tumor cells, had the lowest cytotoxicity index, indicating that this complex also had the highest cytotoxicity toward healthy cells. However, **2** with IC50 values

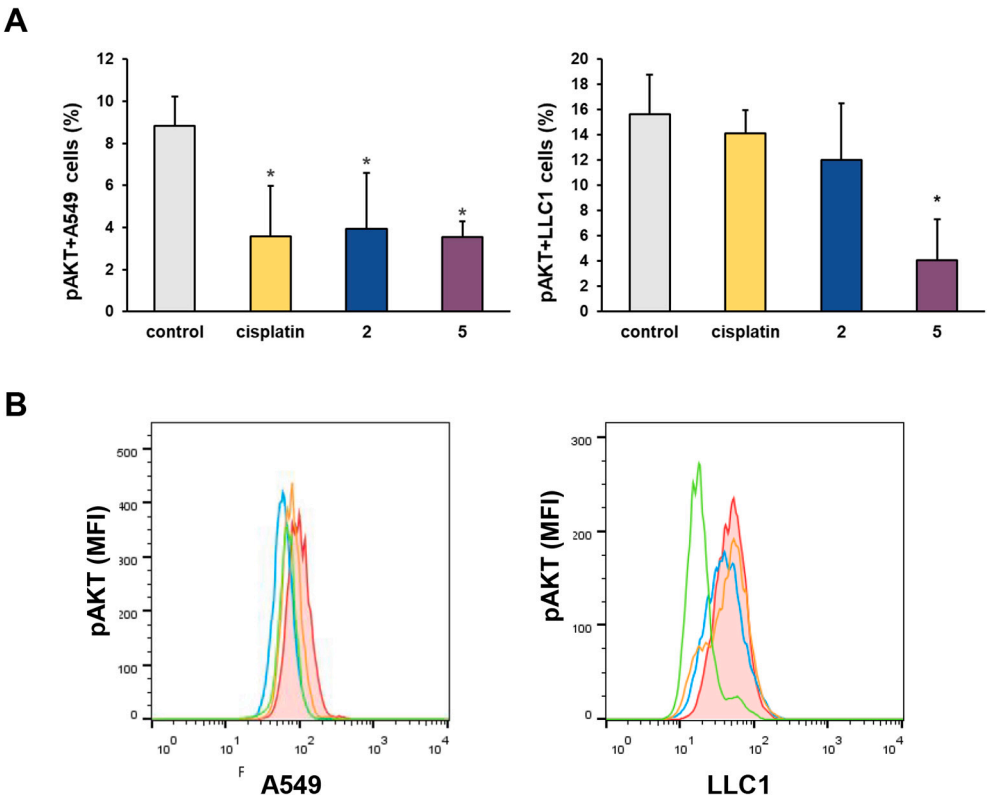

Fig. 13. Ruthenium(III) complexes **2** and **5** decrease the percentage of lung cancer cells that express pAKT. (A) The graphs show the mean + SD for three independent experiments for the percentage of pAKT A549 and LLC1 cells. The statistical significance was determined by the Student's t-test; * $p < 0.05$ indicates the difference in the percentage of treated and untreated cells. (B) Representative histogram of pAKT expression (mean fluorescence intensity) in A549 and LLC1 cells.

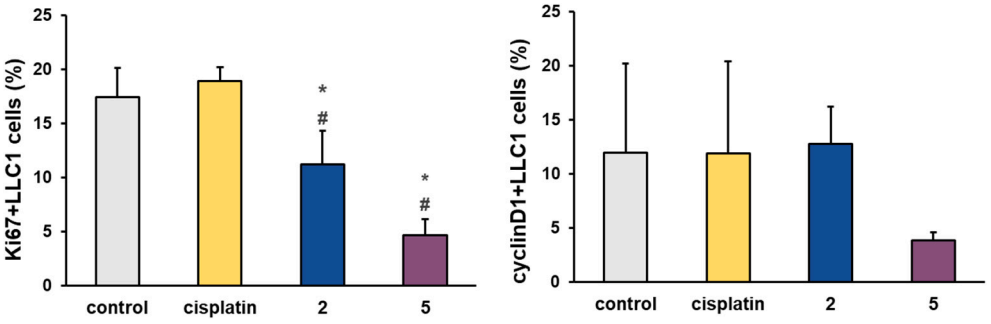

Fig. 14. Ruthenium(III) complexes **2** and **5** decrease the proliferation of LLC1 cells. The graphs show the mean + SD for three independent experiments for the percentage of Ki-67 and cyclin D1 expressing LLC1 cells. The statistical significance was determined by the Student's t-test; * $p < 0.05$ indicates the difference in the percentage of treated and untreated cells; # $p < 0.05$ indicates the difference in the percentage of LLC1 cells Ru- and cisplatin-treated cells.

only slightly higher in comparison with **5** showed the best selectivity index on both tumor cell lines. Based on the findings of better cytotoxic activity of all ruthenium complexes toward lung cancer cell lines, with the lowest IC50 values of **5** and the best selectivity index of **2**, these two complexes were further tested in lung cancer cell lines.

Finally, this finding implied that the aromaticity itself significantly contributed to the anticancer activity of the Ru(III) complexes. Moreover, we demonstrated that the activity of our Ru(III) Schiff base complexes in the studied cells depended on the aromaticity of the tetradentate Schiff base ligand. Introducing the aromatic ring into Schiff base ligand created Ru(III) compounds (**5**) with improved anticancer properties. This observation was also described for the Ru-terpyridyl complexes whose cytotoxicity correlated with the aromaticity of bidentate and *mer* tridentate chelating ligands [33].

3.5.1. *Analysis of the apoptotic potential of ruthenium(III) complexes*

Apoptotic effects of ruthenium complexes have been previously shown in colorectal cancer cell lines [44,45]. In this study, we also used Annexin *V* FITC/PI double staining to measure the apoptotic rate of lung cancer cells treated with **2** and **5** (concentrations of 62.5 μM). Flow cytometry analysis showed that **2** and **5** induced the apoptotic death of A549 cells, with rates higher than for cisplatin (Fig. 10). Complexes **2** and **5** induce the early and late apoptosis of A549 cells in significantly higher percentages in comparison with untreated cells (Fig. 10A). The most of apoptotic A549 cells treated with **2** and **5** were in the phase of early apoptosis (Anenxin V+ PI-). On the other hand, LLC1 cells treated with Ru complexes as well as with cisplatin were in late apoptosis (Annexin V+ PI+). The percentages of LLC1 cells in late apoptosis after the treatment with **2** and **5**, similarly to cisplatin-treated cells, were significantly higher in comparison to untreated cells (Fig. 10B).

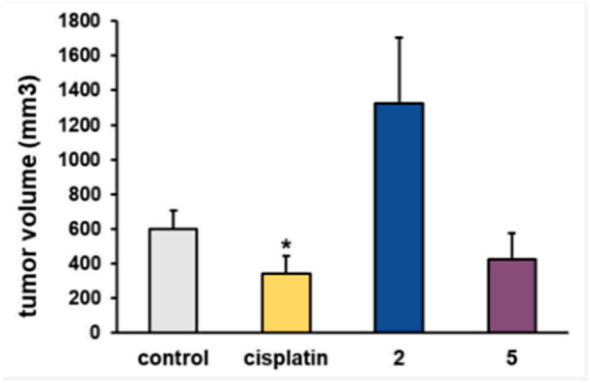

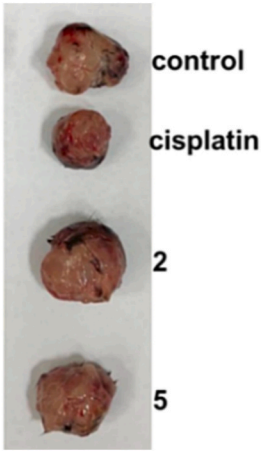

Fig. 15. Complex **5** reduces the growth of primary Lewis lung cancer. Mice (five mice per group) were subcutaneously injected with LLC1 cells, and from the fifteenth day after cell injection, they received either a ruthenium complex, cisplatin, or saline. A) The graphs show the mean values + SD of tumor volume by groups. The statistical significance of the difference was determined by the Student's t-test; * $p < 0.05$ indicates the difference in the percentage of treated and untreated mice; B) The representative dissected tumors from each group.

Table 8
Incidence of metastases in the lungs. The percentage of mice with detected metastases in the lungs was determined 26 days after inoculation of tumor cells in the control group and in groups of mice that received six doses of cisplatin or ruthenium(III) complexes.

	untreated	cisplatin	**2**	**5**
Percentage of mice with lung metastases	100	66.66	33.33	100

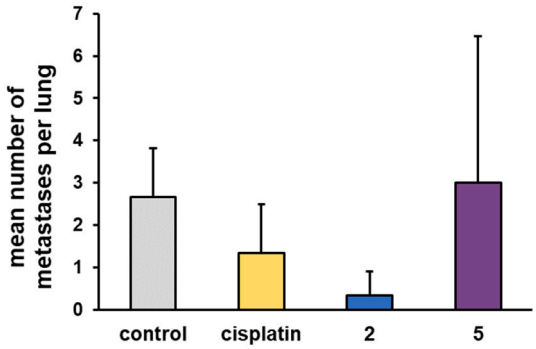

Fig. 16. Complex **2** reduces metastasis in primary heterotopis Lewis lung cancer. The graph presents the mean number of metastases per lung + SD. No statistically significant difference was found between the groups.

Bcl-2 family proteins, by forming heterodimeric complexes at the mitochondria, have an important role in the control of the intrinsic pathway of apoptosis [48]. B-cell lymphoma protein 2 (Bcl-2)-associated X (Bax) protein releases cytochrome *c* from the mitochondria and activates a cascade of caspases that results in cell death. The antiapoptotic protein Bcl-2 prevents Bax mediated releasing of cytochrome *c*, which leads to restriction of apoptotic pathway and cell survival [49]. BH3-only proapoptotic molecule, Noxa binds only Mcl-1 antiapoptotic molecule, and Noxa/Mcl-1 ratio may regulate cell death and survival [50]. Since many cytotoxic agents affect the balance of pro- and anti-apoptotic molecules and thus increase apoptotic cell death, we next analyzed the percentages of Mcl-1 and Noxa expressing A549 and LLC1 cells after treatment with **2** and **5**. We have found a significantly higher percentage of Noxa positive A549 cells treated with **2** and **5** compared to untreated cells and cells treated with cisplatin (Fig. 11A). The percentage of Mcl-1 expressing A549 cells treated with **2** and **5**, and cisplatin was significantly lower in comparison with untreated cells (Fig. 11A). Furthermore, the Mcl-1 to Noxa ratio was significantly lower in the Ru-treated cells in comparison with untreated and cisplatin-treated cells (Fig. 11B). This finding may indicate that **2** and **5** affect the balance between pro- and anti- apoptotic molecules, and thus induce apoptotic death of A549 cells. Complexes **2** and **5** also enhance the expression of proapoptotic Noxa in A549 cells (Fig. 11C).

In LLC1 cells, the treatment with **2** and **5** significantly decreased the percentages of Mcl-1 and Bcl-2 expressing cells (Fig. 12A) but also decreased the percentages of cells that express the proapoptotic molecules Bax and Noxa (Fig. 12B). These complexes also decrease the expression of Mcl1 in LLC1 cells, and increase the expression of Noxa, especially **5** (Fig. 12C). It has been reported that camptothecin enhances the expression of both Noxa and Mcl-1 in HeLa cells, but also induces apoptosis in these cells [50]. This finding is explained by the drug induced altered relative ratio of Mcl-1 and Noxa in the cells that leads them to apoptosis. It is possible that **2** and **5** alter the fine relative ratio of Mcl-1 and Noxa, and thus induce LLC1 apoptosis.

The phosphatidylinositide 3-kinase (PI3K)/AKT-signaling pathway is one of the major survival signals in cancer cells. Phosphorylated, activated AKT inactivates proapoptotic proteins but induces the expression of antiapoptotic proteins, leading to the inhibition of apoptosis [51]. In accordance with the increased Noxa, decreased Mcl-1 and increased apoptosis of A549 cells, we have also found significantly decreased percentages of A549 cells expressing phosphorylated AKT, pAKT, after the treatments with **2** and **5** (Fig. 13A). A significantly lower percentage of pAKT expressing LLC1 was found only after treatment with **5** in comparison with untreated cells (Fig. 13A). Treatment with **5** also induced strong decreases of pAKT expression in LLC1 cells (Fig. 13B). These results may indicate that **2** and **5** induce lung cancer cell death (A549 cells) by inhibition of AKT activation, which results in the decrease of expression of Mcl-1, an important protein for lung cancer survival and therapy resistance [52], and an altered Mcl-1 to Noxa ratio, ultimately leading to apoptosis.

3.5.2. Ruthenium(III) complexes reduce the percentage of proliferative LLC1 cells

Ruthenium(III) complexes **2** and **5** significantly reduce the percentage of LLC1 cells expressing Ki-67 in comparison with untreated and cells treated with cisplatin (Fig. 14). Additionally, **5** reduced the percentage of cyclin D1 expressing LLC1 cells, but this decrease was not statistically significant (Fig. 14). Ki-67 is a protein expressed in the nucleus of proliferating cells and is a one of the key markers of aggressive proliferation of cancer cells and poor prognosis [53]. Probably, ruthenium(III) complexes exert their antitumor activity partly by reducing the proliferation of LLC1 cells.

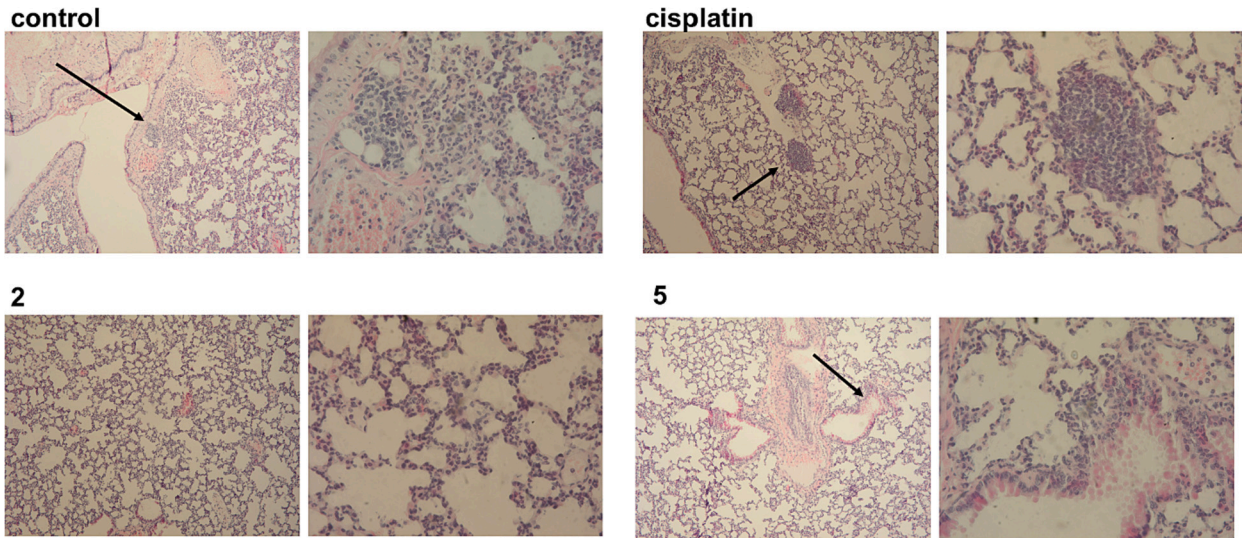

Fig. 17. Representative lung tissue sections stained with hematoxylin and eosin 26 days after LLC1 cell subcutaneous injection (magnification 100× and 400×).

3.6. *In vivo studies*

3.6.1. *Complex **5** reduces Lewis lung cancer growth*

In light of the results obtained in testing the cytotoxic effects of **2** and **5** in vitro, our next goal was to explore the potential of the tested complexes to reduce the growth and metastasis of murine Lewis lung cancer in vivo. LLC1 cells were injected subcutaneously into the flank of the mice, and the 15th day of appearance of a palpable tumor, the treatment with **2** and **5**, and cisplatin as a control substance, started. **5** reduced the tumor volume calculated after necropsy, while this reduction of volume was significant in a group of cisplatin-treated mice (Fig. 15). Tumors in the complex **2**-treated group of mice were larger and had higher volumes compared to the control group of mice.

3.6.2. *Complex **2** reduces lung metastasis in mice with primary Lewis lung cancer*

Lung tissues were analyzed 26 days after the tumor cell inoculation in the groups of untreated, mice that received **2**, **5**, or cisplatin intraperitoneally. Histological analysis of five serial slides of lung tissue revealed that **2** reduced the incidence of lung metastases, while all mice treated with **5** developed metastases in the lung (Table 8).

Moreover, complex **2** significantly reduced the mean number of metastases per lung in comparison with untreated and mice treated with cisplatin (Fig. 16). Complex **2**, although it does not reduce the growth of the primary tumor, showed better antimetastatic activity compared to cisplatin.

There were no well-formed metastatic foci in the lungs of complex **5**-treated mice, as was seen in the mice treated with cisplatin (Fig. 17). Also, in the lungs of mice treated with **5** metastases, there were hyperemia and hemorrhages (Fig. 17). Small foci of hemorrhages were detected in the lungs of complex **2**-treated mice, but no metastases were detected in any lung section.

4. Conclusion

Ruthenium compounds containing Schiff base ligands represent a novel family of promising metal-based pharmaceuticals with a variety of potential therapeutic applications, notably for anticancer and antimicrobial treatments. In the current research, we described the synthesis and structural characterization of a series of new ruthenium(III) complexes (**1–6**) with the tetradentate ligands, alongside with their interactions with the biomolecules DNA and BSA. Herein, we also present the anticancer activity of the complexes against human and mouse lung adenocarcinoma (A549 and LLC1) and colorectal cancer (HCT116 and CT26), respectively. Complexes **2** and **5**, as the most promising anticancer compounds, were further tested in vivo on a heterotopic model of murine Lewis lung cancer (LLC1).

A study of the interaction of **1–6** with CT DNA demonstrated that complexes with aromatic ligands (**2** and **5**) showed the most efficient competition with EB in binding to CT DNA, indicating that the reduced number of aromatic rings or their absence caused lower intercalative properties of the complexes. On the other hand, the Hoechst-quenching experiments clearly demonstrated the greatest ability of complexes with non-aromatic ligands (**1** and **4**) to displace Hoechst molecules linked to CT DNA, suggesting the minor groove as the preferred mode of binding. A molecular docking study was consistent with the experimentally obtained results, revealing that the binding affinity to DNA increases with increasing surface area and/or hydrophobicity of the complex in the order: **1** > **4** > **3** > **6** > **5** > **2**.

Additionally, we examined the interaction of **1–6** with BSA in the presence and absence of markers for site I of subdomain IIA (eosin Y) and for site II of subdomain IIIA (ibuprofen). Ru complexes bind to IIA and IIIA sites with moderate binding affinity with similar K_b values ($K_b = 10^4\ M^{-1}$). Interestingly, from the molecular docking study, based on the more negative ΔG_{bind} and low K_i values, it can be concluded that all newly synthesized compounds exhibit the highest binding affinity for active site III, a third *D*-shaped hydrophobic pocket for drug binding within subdomain IB.

Moreover, complexes **2** and **5** exert a considerable antitumor effect in vitro and a modest antitumor effect in vivo in the model of mouse heterotopic primary Lewis lung cancer. Complex **5** reduced the volume of mouse primary heterotopic Lewis lung cancer, while **2** reduced the incidence and mean number of metastases per lung. This investigation is significant for the further design and development of new organometallic compounds as therapeutic agents with unique properties that intermediate between those of classical inorganic and organic materials.

CRediT authorship contribution statement

Milica Međedović: Investigation, Validation, Writing – original draft. **Aleksandar Mijatović:** Investigation, Validation. **Rada Baošić:** Investigation, Validation, Methodology. **Dejan Lazić:** Investigation, Data curation, Methodology. **Žiko Milanović:** Investigation, Software, Writing – original draft. **Zoran Marković:** Investigation, Software, Methodology. **Jelena Milovanović:** Investigation, Methodology, Writing – original draft. **Dragana Arsenijević:** Investigation,

Methodology. **Bojana Stojanović:** Investigation, Methodology. **Miloš Arsenijević:** Investigation, Methodology. **Marija Milovanović:** Investigation, Methodology, Writing – original draft. **Biljana Petrović:** Data curation, Investigation, Methodology, Validation. **Ana Rilak Simović:** Supervision, Validation, Methodology, Writing – review & editing.

Author statement

This is a statement to certify that all authors have seen and approved the final version of the manuscript being submitted. The article is the authors' original work, has not received prior publication and is not under consideration for publication elsewhere.

Declaration of Competing Interest

There are no conflicts to declare.

Data availability

Data will be made available on request.

Acknowledgment

The authors would like to express their gratitude to the Ministry of Science, Technological Development and Innovation of the Republic of Serbia (Agreement No. 451-03-47/2023-01/200378, Agreement No. 451-03-47/2023-01/200122 and Agreement No. 451-03-47/2023-01/200111) for financial support. Additionally, A.R.S. thanks to Dr. Dušan Milivojević from the Institute of Nuclear Science Vinča, Laboratory of Radiation Chemistry and Physics for recording and analyzing the EPR spectra.

Appendix A. Supplementary data

Supplementary data to this article can be found online at https://doi.org/10.1016/j.jinorgbio.2023.112363.

References

[1] S. Parveen, Recent advances in anticancer ruthenium Schiff base complexes, Appl. Organomet. Chem. 34 (2020) 1–23, https://doi.org/10.1002/aoc.5687.
[2] A. Hameed, M. Al-Rashida, M. Uroos, S. Abid Ali, K.M. Khan, Schiff bases in medicinal chemistry: a patent review (2010-2015), Expert Opin. Ther. Pat. 27 (2017) 63–79, https://doi.org/10.1080/13543776.2017.1252752.
[3] L.P.K. Ang, D.T.H. Tan, T.T. Phan, J. Li, R. Beuerman, R.M. Lavker, The in vitro and in vivo proliferative capacity of serum-free cultivated human conjunctival epithelial cells, Curr. Eye Res. 28 (2004) 307–317, https://doi.org/10.1076/ceyr.28.5.307.28677.
[4] M. Lashanizadegan, M. Jamshidbeigi, h c r e v i f o, J. Dermatol. Sci. 22 (2011) 121–124.
[5] I.P. Ejidike, P.A. Ajibade, Transition metal complexes of symmetrical and asymmetrical Schiff bases as antibacterial, antifungal, antioxidant, and anticancer agents: Progress and prospects, Rev. Inorg. Chem. 35 (2015) 191–224, https://doi.org/10.1515/revic-2015-0007.
[6] M.K. Mohamed Subarkhan, L. Ren, B. Xie, C. Chen, Y. Wang, H. Wang, Novel tetranuclear ruthenium(II) arene complexes showing potent cytotoxic and antimetastatic activity as well as low toxicity in vivo, Elsevier Masson SAS (2019), https://doi.org/10.1016/j.ejmech.2019.06.061.
[7] J.J.O. and A.E. martell Richard J. Hovey, Inner complex chelates. 11. Analogs and polar substituted analogs of Bisacetylacetoneethylenediimine and its metal chelates, J. Am. Chem. Soc. 81 (1958) 3189.
[8] F. Dimiza, S. Fountoulaki, A.N. Papadopoulos, C.A. Kontogiorgis, V. Tangoulis, C. P. Raptopoulou, V. Psycharis, A. Terzis, D.P. Kessissoglou, G. Psomas, Non-steroidal antiinflammatory drug-copper(II) complexes: structure and biological perspectives, Dalton Trans. 40 (2011) 8555–8568, https://doi.org/10.1039/c1dt10714c.
[9] S. Stoll, A. Schweiger, EasySpin, a comprehensive software package for spectral simulation and analysis in EPR, J. Magn. Reson. 178 (2006) 42–55, https://doi.org/10.1016/j.jmr.2005.08.013.
[10] M.F.S. Garrett, M. Morris, Ruth Huey, William Lindstrom, A.J.O. Richard, K. Belew, David S. Goodsell, AutoDock4 and AutoDockTools4: automated docking with selective receptor flexibility, J. Comput. Chem. 30 (2009) 2785–2791, https://doi.org/10.1002/jcc.
[11] M.J. Frisch, G.W. Trucks, H.B. Schlegel, G.E. Scuseria, M.A. Robb, J.R. Cheeseman, G. Scalmani, V. Barone, B. Mennucci, G.A. Petersson, H. Nakatsuji, M. Caricato, X. Li, H.P. Hratchian, A.F. Izmaylov, J. Bloino, G. Zheng, J.L. Sonnenberg, M. Hada, M. Ehara, K. Toyota, R. Fukuda, J. Hasegawa, M. Ishida, T. Nakajima, Y. Honda, O. Kitao, H. Nakai, T. Vreven, J.A. Montgomery Jr., J.E. Peralta, F. Ogliaro, M. Bearpark, J.J. Heyd, E. Brothers, K.N. Kudin, V.N. Staroverov, R. Kobayashi, J. Normand, K. Raghavachari, A. Rendell, J.C. Burant, S.S. Iyengar, J. Tomasi, M. Cossi, N. Rega, J.M. Millam, M. Klene, J.E. Knox, J.B. Cross, V. Bakken, C. Adamo, J. Jaramillo, R. Gomperts, R.E. Stratmann, O. Yazyev, A.J. Austin, R. Cammi, C. Pomelli, J.W. Ochterski, R.L. Martin, K. Morokuma, V.G. Zakrzewski, G.A. Voth, P. Salvador, J.J. Dannenberg, S. Dapprich, A.D. Daniels, Ö. Farkas, J. B. Foresman, J.V. Ortiz, J. Cioslowski, D.J. Fox, Gaussian09 Revision D.01, 2023.
[12] Y. Zhao, N.E. Schultz, D.G. Truhlar, M052X, J. Chem. Theory Comput. 2 (2006) 364–382. http://pubs.acs.org/doi/abs/10.1021/ct0502763.
[13] A.D. Becke, E.R. Johnson, A density-functional model of the dispersion interaction, J. Chem. Phys. 123 (2005), 154101, https://doi.org/10.1063/1.2065267.
[14] A. Bujacz, Structures of bovine, equine and leporine serum albumin, Acta Crystallogr. Sect. D Biol. Crystallogr. 68 (2012) 1278–1289, https://doi.org/10.1107/S0907444912027047.
[15] A J.A. and M.C. Albert Canals, Monica Purciolas, The anticancer agent ellipticine unwinds DNA by intercalative binding in an orientation parallel to base pairs, Biol. Crystallogr. 61 (2005) 1009–1012, https://doi.org/10.1107/S0907444905015404.
[16] H.R. Drewt, R.M. Wingtt, T. Takanot, C. Brokat, S. Tanakat, K. Itakuraii, R. E. Dickersont, Structure of a B-DNA dodecamer: conformation and dynamics *, Biochemistry 78 (1981) 2179–2183.
[17] Z.S. Edina, H. Avdovića, Žiko B. Milanović, Marko N. Živanovića, Dragana S. Šeklića, Ivana D. Radojevića, Ljiljana R. Čomić, Srećko R. Trifunović, Ana Amić, Markovića, Synthesis, spectroscopic characterization, biological activity, DFT and molecular docking study of novel 4-hydroxycoumarine derivatives and corresponding palladium(II) complexes, Inorg. Chim. Acta (2020), 119465, https://doi.org/10.1016/j.ica.2020.119465.
[18] D. Milenković, E. Avdović, D. Dimić, S. Sudha, D. Ramarajan, Ž. Milanović, S. Trifunović, Z.S. Marković, Vibrational and Hirshfeld surface analyses, quantum chemical calculations, and molecular docking studies of coumarin derivative 3-(1-m-toluidinoethylidene)-chromane-2,4-dione and its corresponding palladium(II) complex, J. Mol. Struct. (2020), 127935, https://doi.org/10.1016/j.molstruc.2020.127935.
[19] Ikechukwu P. Ejidike, Peter A. Ajibade, Synthesis, Characterization and Biological Studies of Metal(II) Complexes of (3E)-3-[(2-{(E)-[1-(2,4-Dihydroxyphenyl) ethylidene]amino}ethyl)imino]-1-phenylbutan-1-one Schiff Base 20, 2015, pp. 9788–9802, https://doi.org/10.3390/molecules20069788.
[20] R. Karvembu, K. Natarajan, Synthetic, catalytic and biological studies of new binuclear ruthenium(II) complexes containing thiobis(β-diketones) and triphenylphosphine, Polyhedron. 21 (2002) 1721–1727, https://doi.org/10.1016/S0277-5387(02)01038-0.
[21] K.N. Kumar, R. Ramesh, Y. Liu, Synthesis, structure and catalytic activity of cycloruthenated carbonyl complexes containing arylazo phenolate ligands, J. Mol. Catal. A Chem. 265 (2007) 218–226, https://doi.org/10.1016/j.molcata.2006.10.015.
[22] K.P. Balasubramanian, R. Karvembu, R. Prabhakaran, V. Chinnusamy, K. Natarajan, Synthesis, spectral, catalytic and antimicrobial studies of PPh3/AsPh3 complexes of Ru(II) with dibasic tridentate O, N, S donor ligands, Spectrochim. Acta Part A Mol. Biomol. Spectrosc. 68 (2007) 50–54, https://doi.org/10.1016/j.saa.2006.10.049.
[23] I.P. Ejidike, P.A. Ajibade, Synthesis, characterization, and in vitro antioxidant and anticancer studies of ruthenium(III) complexes of symmetric and asymmetric tetradentate Schiff bases, J. Coord. Chem. 68 (2015) 2552–2564, https://doi.org/10.1080/00958972.2015.1043127.
[24] G. Venkatachalam, R. Ramesh, Catalytic and biological activities of Ru(III) mixed ligand complexes containing N,O donor of 2-hydroxy-1-naphthylideneimines, Spectrochim. Acta Part A Mol. Biomol. Spectrosc. 61 (2005) 2081–2087, https://doi.org/10.1016/j.saa.2004.08.008.
[25] T.D. Thangadurai, K. Natarajan, New ruthenium(III) complexes containing tetradentate Schiff bases and their antibacterial activity, Transit. Met. Chem. 25 (2000) 347–351, https://doi.org/10.1023/A:1007028431330.
[26] C.A. Bolos, A.T. Chaviara, D. Mourelatos, Z. Iakovidou, E. Mioglou, E. Chrysogelou, A. Papageorgiou, Synthesis, characterization, toxicity, cytogenetic and in vivo antitumor studies of 1,1-dithiolate cu(II) complexes with di-, tri-, tetra- amines and 1,3-thiazoles. Structure-activity correlation, Bioorg. Med. Chem. 17 (2009) 3142–3151, https://doi.org/10.1016/j.bmc.2009.02.059.
[27] T.T. Thai, B. Therrien, G. Süss-Fink, Pentamethylcyclopentadienyl rhodium and iridium complexes containing oxinato ligands, Inorg. Chem. Commun. 12 (2009) 806–807, https://doi.org/10.1016/j.inoche.2009.06.023.
[28] R. Payne, P. Govender, B. Therrien, C.M. Clavel, P.J. Dyson, G.S. Smith, Neutral and cationic multinuclear half-sandwich rhodium and iridium complexes coordinated to poly(propyleneimine) dendritic scaffolds: synthesis and cytotoxicity, J. Organomet. Chem. 729 (2013) 20–27, https://doi.org/10.1016/j.jorganchem.2013.01.009.
[29] P. Govindaswamy, B. Therrien, G. Süss-Fink, P. Štěpnička, J. Ludvík, Mono and dinuclear iridium, rhodium and ruthenium complexes containing chelating carboxylato pyrazine ligands: synthesis, molecular structure and electrochemistry, J. Organomet. Chem. 692 (2007) 1661–1671, https://doi.org/10.1016/j.jorganchem.2006.12.040.

[30] M. Fandzloch, A. Wojtczak, J. Sitkowski, I. Łakomska, Interaction of ruthenium(II) and ruthenium(III) ions with 5-methyl-1,2,4-triazolo[1,5-a]pyrimidin-7(4H)-one, Polyhedron. 67 (2014) 410–415, https://doi.org/10.1016/j.poly.2013.09.022.
[31] L. Zeng, P. Gupta, Y. Chen, E. Wang, L. Ji, H. Chao, Z.S. Chen, The development of anticancer ruthenium(II) complexes: from single molecule compounds to nanomaterials, Chem. Soc. Rev. 46 (2017) 5771–5804, https://doi.org/10.1039/c7cs00195a.
[32] T. Lazarević, A. Rilak, Ž.D. Bugarčić, Platinum, palladium, gold and ruthenium complexes as anticancer agents: current clinical uses, cytotoxicity studies and future perspectives, Eur. J. Med. Chem. 142 (2017) 8–31, https://doi.org/10.1016/j.ejmech.2017.04.007.
[33] A. Rilak Simović, R. Masnikosa, I. Bratsos, E. Alessio, Chemistry and reactivity of ruthenium(II) complexes: DNA/protein binding mode and anticancer activity are related to the complex structure, Coord. Chem. Rev. 398 (2019), 113011, https://doi.org/10.1016/j.ccr.2019.07.008.
[34] M. Pavlović, E. Kahrović, S. Aranđelović, S. Radulović, P.P. Ilich, S. Grgurić-Šipka, N. Ljubijankić, D. Žilić, J. Jurec, Tumor selective Ru(III) Schiff bases complexes with strong in vitro activity toward cisplatin-resistant MDA-MB-231 breast cancer cells, J. Biol. Inorg. Chem. (2023), https://doi.org/10.1007/s00775-023-01989-0.
[35] V. Brabec, J. Kasparkova, Ruthenium coordination compounds of biological and biomedical significance. DNA binding agents, Coord. Chem. Rev. 376 (2018) 75–94, https://doi.org/10.1016/j.ccr.2018.07.012.
[36] H.J. Yin, A.G. Zhang, L.H. Gao, H. Zhao, K.Z. Wang, DNA groove-binding and acid-base properties of a Ru(II) complex containing anthryl moieties, Nucleosides Nucleotides Nucleic Acids 39 (2020) 592–614, https://doi.org/10.1080/15257770.2019.1669804.
[37] J. Sun, Y. Huang, C. Zheng, Y. Zhou, Y. Liu, J. Liu, Ruthenium (II) complexes interact with human serum albumin and induce apoptosis of tumor cells, Biol. Trace Elem. Res. 163 (2015) 266–274, https://doi.org/10.1007/s12011-014-0165-7.
[38] S. Maikoo, B. Xulu, A. Mambanda, N. Mkhwanazi, C. Davison, J.A. de la Mare, I. N. Booysen, Biomolecular interactions of cytotoxic ruthenium compounds with Thiosemicarbazone or Benzothiazole Schiff Base chelates, ChemMedChem. 17 (2022), https://doi.org/10.1002/cmdc.202200444.
[39] D.C. Carter, J.X. Ho, Structure of serum albumin, in: Adv. Protein Chem, Marshall Space Fllght Center, Huntsville, Alabama, Alabama, 1994, pp. 153–176, https://doi.org/10.1016/S0065-3233(08)60640-3.
[40] X.Z. Feng, Z. Lin, L.J. Yang, C. Wang, C. Li Bai, Investigation of the interaction between acridine orange and bovine serum albumin, Talanta. 47 (1998) 1223–1229, https://doi.org/10.1016/S0039-9140(98)00198-2.
[41] H.A. Alhazmi, FT-IR spectroscopy for the identification of binding sites and measurements of the binding interactions of important metal ions with bovine serum albumin, Sci. Pharm. 87 (2019) 5, https://doi.org/10.3390/scipharm87010005.
[42] O.A. Chaves, L.B. Menezes, B.A. Iglesias, Multiple spectroscopic and theoretical investigation of meso-tetra-(4-pyridyl)porphyrin-ruthenium(II) complexes in HSA-binding studies. Effect of Zn(II) in protein binding, J. Mol. Liq. 294 (2019), 111581, https://doi.org/10.1016/j.molliq.2019.111581.
[43] K.M. Mahmud, M.S. Niloy, M.S. Shakil, M.A. Islam, Ruthenium complexes: an alternative to platinum drugs in colorectal cancer treatment, Pharmaceutics. 13 (2021) 1295, https://doi.org/10.3390/pharmaceutics13081295.
[44] N. Ribeiro, P.F. Farinha, J.O. Pinho, H. Luiz, J.P. Mészáros, A.M. Galvão, J. Costa Pessoa, É.A. Enyedy, C.P. Reis, I. Correia, M.M. Gaspar, Metal coordination and biological screening of a Schiff base derived from 8-hydroxyquinoline and benzothiazole, Pharmaceutics. 14 (2022) 1–29, https://doi.org/10.3390/pharmaceutics14122583.
[45] I. Vivo, M. Savic, A. Arsenijevic, J. Milovanovic, B. Stojanovic, Complexes towards Colon Cancer Cells In Vitro and, Molecules 4699, 2020, pp. 2–20.
[46] Q. Sun, Y. Li, H. Shi, Y. Wang, J. Zhang, Q. Zhang, Ruthenium complexes as promising candidates against lung cancer, Molecules. 26 (2021), https://doi.org/10.3390/molecules26154389.
[47] A. Păucean, V. Mureșan, S. Maria-Man, M.S. Chiș, A.E. Mureșan, L.R. Șerban, A. Pop, S. Muste, Metabolomics as a tool to elucidate the sensory, nutritional and safety quality of wheat bread—a review, Int. J. Mol. Sci. 22 (2021), https://doi.org/10.3390/ijms22168945.
[48] Shimizu Shigeomi, Narita Masashi, Tsujimoto Yoshihide, Bcl-2 family proteins regulate the release of apoptogenic cytochrome c by the mitochondrial channel VDAC, Nature 399 (1999) 1–5. https://vpn.uibk.ac.at/+CSCO+10756767633A2F2F6A6A6A2E616E676865722E70627A++/articles/20959.pdf.
[49] R.J. Youle, A. Strasser, The BCL-2 protein family: opposing activities that mediate cell death, Nat. Rev. Mol. Cell Biol. 9 (2008) 47–59, https://doi.org/10.1038/nrm2308.
[50] Y. Mei, C. Xie, W. Xie, X. Tian, M. Li, M. Wu, Noxa/Mcl-1 balance regulates susceptibility of cells to camptothecin-induced apoptosis, Neoplasia. 9 (2007) 871–881, https://doi.org/10.1593/neo.07589.
[51] C.S. Mitsiades, N. Mitsiades, V. Poulaki, R. Schlossman, M. Akiyama, D. Chauhan, T. Hideshima, S.P. Treon, N.C. Munshi, P.G. Richardson, K.C. Anderson, Activation of NF-KB and upregulation of intracellular anti-apoptotic proteins via the IGF-1/Akt signaling in human multiple myeloma cells: therapeutic implications, Oncogene. 21 (2002) 5673–5683, https://doi.org/10.1038/sj.onc.1205664.
[52] Y. Sakuma, S. Hirai, T. Sumi, M. Tada, T. Kojima, T. Niki, M. Yamaguchi, MCL1 inhibition enhances the efficacy of docetaxel against airway-derived squamous cell carcinoma cells, Exp. Cell Res. 406 (2021), 112763, https://doi.org/10.1016/j.yexcr.2021.112763.
[53] R. Rahmanzadeh, P. Rai, J.P. Celli, I. Rizvi, B. Baron-Lühr, J. Gerdes, T. Hasan, Ki-67 as a molecular target for therapy in an in vitro three-dimensional model for ovarian cancer, Cancer Res. 70 (2010) 9234–9242, https://doi.org/10.1158/0008-5472.CAN-10-1190.